

Downlink and Uplink Cooperative Joint Communication and Sensing

Xu Chen, *Student Member, IEEE*, Zhiyong Feng, *Senior Member, IEEE*, J. Andrew Zhang, *Senior Member, IEEE*, Zhiqing Wei, *Member, IEEE*, Xin Yuan, *Member, IEEE*, and Ping Zhang, *Fellow, IEEE*

Abstract—Downlink (DL) and uplink (UL) joint communication and sensing (JCAS) technologies have been individually studied for realizing sensing using DL and UL communication signals, respectively. Since the spatial environment and JCAS channels in the consecutive DL and UL JCAS time slots are generally unchanged, DL and UL JCAS can be jointly designed to achieve better sensing and communication performance. In this paper, we propose a novel DL and UL cooperative (DUC) JCAS scheme, including a unified multiple signal classification (MUSIC)-based JCAS sensing scheme for both DL and UL JCAS and a DUC JCAS fusion method. The unified MUSIC JCAS sensing scheme can accurately estimate angle-of-arrival (AoA), range, and Doppler based on a unified MUSIC-based sensing module. The DUC JCAS fusion method can distinguish between the sensing results of the communication user and other dumb targets. Moreover, by exploiting the channel reciprocity, it can also improve the sensing and channel state information (CSI) estimation accuracy. Extensive simulation results validate the proposed DUC JCAS scheme. It is shown that the minimum location and velocity estimation mean square errors of the proposed DUC JCAS scheme are about 20 dB lower than those of the state-of-the-art separated DL and UL JCAS schemes.

Index Terms—Joint communication and sensing, 6G networks, downlink and uplink cooperation.

I. INTRODUCTION

A. Existing Research and Motivations

Wireless communication and sensing capabilities are both indispensable for the 6th generation (6G) machine-type applications, e.g., intelligent vehicular networks, manufacturing, and smart cities [1], [2]. Unfortunately, the proliferation of wireless sensing and communication nodes has resulted in severe spectrum congestion problems [3]. In this context, the joint communication and sensing (JCAS) technology has emerged as one of the most promising 6G key technologies. It aims to achieve wireless sensing and communication abilities simultaneously using unified spectrum and transceivers, sharing the same transmitted signals [4].

Xu Chen, Z. Feng, and Z. Wei are with Beijing University of Posts and Telecommunications, Key Laboratory of Universal Wireless Communications, Ministry of Education, Beijing 100876, P. R. China (Email: {chenxu96330, fengzy, weizhiqing}@bupt.edu.cn).

J. A. Zhang is with the Global Big Data Technologies Centre, University of Technology Sydney, Sydney, NSW, Australia (Email: Andrew.Zhang@uts.edu.au).

Ping Zhang is with Beijing University of Posts and Telecommunications, State Key Laboratory of Networking and Switching Technology, Beijing 100876, P. R. China (Email: pzhang@bupt.edu.cn).

X. Yuan is with Commonwealth Scientific and Industrial Research Organization (CSIRO), Australia (email: Xin.Yuan@data61.csiro.au).

Corresponding author: Zhiyong Feng

Up to now, downlink (DL) and uplink (UL) JCAS utilized in mobile networks have been widely studied, adapting to the DL and UL transmission modes of communication systems, respectively. Sturm *et al.* [5] proposed an orthogonal frequency-division multiplexing (OFDM)-based JCAS signal processing method, which satisfies both the active range detection and communication requirements by using the echoes of communication signals. Zhang *et al.* [6] proposed a practical OFDM time-division-duplex (TDD) multibeam scheme to achieve JCAS that is suitable for DL echo sensing, which complies with the prevalent terrestrial packet communication system. As pointed out in [7], the critical enabler for implementing DL JCAS is the full-duplex (FD) operation to transmit JCAS signals and receive reflections simultaneously. Seyed Ali *et al.* [8] realized an FD JCAS platform that detects targets while communicating with another node by canceling the self-leakage interference with analog and digital self-leakage canceler. In [9], the authors studied spatio-temporal power optimization problems for multi-input multi-output (MIMO) DL JCAS system. In [10], the authors proposed a UL JCAS method for perceptive mobile networks, allowing a static user and base station (BS) to form a bi-static system to sense the environment. Liu *et al.* [11] proposed that super-resolution sensing method can be used to achieve DL active range and Doppler estimation. In [12], the authors proposed a refined multiple signal classification (MUSIC)-based JCAS sensing scheme to achieve accurate estimation of the angle of arrival (AoA), range and velocity. All the above researches have laid fundamentals for implementing both the DL mono-static JCAS that exploits the echoes of DL signals, and UL bi-static JCAS that utilizes the UL signals.

In the consecutive UL and DL time slots, the spatial parameters of the environment can be treated as unchanged, which leads to the channel reciprocity [3]. The JCAS operations in consecutive UL and DL time slots can be treated as independent estimates of highly correlated sensing parameters. UL and DL JCAS can potentially be jointly processed to improve the communication and sensing performance of the entire JCAS system. However, few studies have studied the cooperation between UL and DL JCAS up to now.

B. Contributions

Taking advantage of the above potential in achieving cooperation between the UL and DL JCAS processes, we propose a DL and UL cooperative (DUC) JCAS processing scheme for OFDM-based systems, which can improve the sensing

accuracy and communication reliability. This scheme consists of a unified DUC super-resolution sensing method and a DUC JCAS data fusion method. The unified DUC super-resolution sensing method can use the same MUSIC-based JCAS sensing module to accurately estimate AoA, range, and velocity for both UL bi-static and DL mono-static sensing. Specifically, the unknown AoA and range of the user equipment (UE) can be estimated in the UL JCAS, and this prior information can be exploited in the DL JCAS processing via beamforming (BF) for effective interference mitigation between communication and sensing. The DUC JCAS data fusion method integrates the UL and DL JCAS sensing results to distinguish between the sensing results of the communication user and other dumb scatterers, and to improve the sensing accuracy. Besides, it fuses the UL and DL channel state information (CSI) to improve communication reliability.

The main contributions of this paper are summarized as follows.

1. We propose a DUC JCAS processing scheme that uses a common refined two-dimensional (2D) MUSIC algorithm for estimating AoA, range, and velocity for both UL and DL sensing. The estimated UE's AoA and range in UL JCAS can offer crucial prior information for JCAS BF in DL JCAS processing, which leads to efficient interference mitigation between DL sensing and communication.
2. We propose a DUC JCAS fusion method by leveraging the correlation between UL and DL JCAS channels. It can distinguish the sensing results of the communication user from the other dumb targets, and improve the sensing estimation accuracy by integrating the UL and DL JCAS processing results.
3. We propose a DUC JCAS CSI fusion method that can integrate the CSI estimates from both UL and DL channel estimation to reduce the error in CSI estimation by exploiting the channel reciprocity of mobile networks.

Extensive simulations are conducted to validate the proposed DUC JCAS scheme. The simulation results show that the location and velocity estimation mean square errors (MSEs) of the proposed DUC JCAS scheme are about 20 dB lower than the state-of-the-art separated DL and UL JCAS schemes. The communication CSI enhancement can improve the bit error rate (BER) performance. The remaining parts of this paper are organized as follows. In section II, we describe the system model for the DUC JCAS scheme. Section III proposes the DUC JCAS sensing processing scheme. Section IV proposes the DUC JCAS fusion method. In section V, the simulation results are presented. Section VI concludes this paper.

Notations: Bold uppercase letters denote matrices (e.g., \mathbf{M}); bold lowercase letters denote column vectors (e.g., \mathbf{v}); scalars are denoted by normal font (e.g., γ); the entries of vectors or matrices are referred to with square brackets, for instance, the q th entry of vector \mathbf{v} is $[\mathbf{v}]_q$, and the entry of the matrix \mathbf{M} at the m th row and q th column is $[\mathbf{M}]_{n,m}$; $\mathbf{U}_s = [\mathbf{U}]_{:,N_1:N_2}$ means the matrices sliced from the N_1 th to the N_2 th columns of \mathbf{U} ; $(\cdot)^H$, $(\cdot)^*$ and $(\cdot)^T$ denote Hermitian transpose, complex conjugate and transpose, respectively; $\|\mathbf{v}_k\|_l$ represents the l -

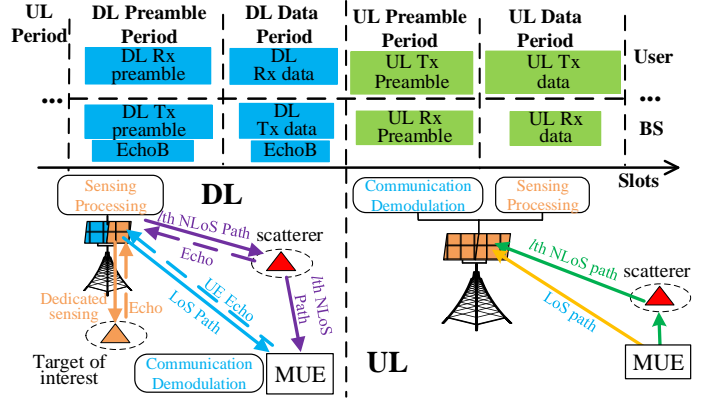


Fig. 1: The DUC JCAS scenario.

norm of \mathbf{v}_k , and ℓ_2 -norm is considered in this paper; $\text{eig}(\mathbf{M})$ is the eigenvalue decomposition of \mathbf{M} , and $E(\cdot)$ represents the expectation of random variables; $\mathbf{M}_1 \in \mathbb{C}^{M \times N}$ and $\mathbf{M}_2 \in \mathbb{R}^{M \times N}$ are $M \times N$ complex-value and real-value matrices, respectively; and $v \sim \mathcal{CN}(m, \sigma^2)$ means v follows a circular symmetric complex Gaussian (CSCG) distribution with mean m and variance σ^2 .

II. SYSTEM MODEL

This section presents the DUC JCAS system setup, JCAS channel models, and transmit and received signal models to provide fundamentals for DUC JCAS signal processing.

A. DUC JCAS System Setup

We consider a DUC JCAS scenario, where the user and BS conduct alternating DL and UL JCAS operations, as shown in Fig. 1. A multipath channel model is considered for the block fading channel. Millimeter-wave (mmWave) and uniform plane arrays (UPAs) are used for the DUC JCAS system. The BS is equipped with two spatially well-separated UPAs and self-leakage canceler to transmit JCAS signals and receive reflections simultaneously, as developed in [8]. Moreover, synchronization between the BS and user is achieved via a global clock, such as GPS. The clock between them is assumed to be locked, as discussed in [13]. Thus, the timing and carrier frequency residual offset are neglected in the signal model.

In the UL preamble (ULP) period, the user transmits the ULP signal, and BS receives it for both UL communication setting such as channel estimation and estimating the user's sensing parameters in a bi-static manner. In the UL data (ULD) period, the BS receives and demodulates the ULD signal. In the DL preamble (DLP) period, the user receives the DLP signal from BS for synchronization and channel estimation. BS does not operate JCAS in the DLP period to ensure the best channel estimation. In the DL data (DLD) period, BS transmits the DLD signal to the user and sensing probe signal to the direction-of-interest (DoI), and simultaneously receives the echo signals from both the direction-of-user (DoU) and DoI to perform mono-static sensing.

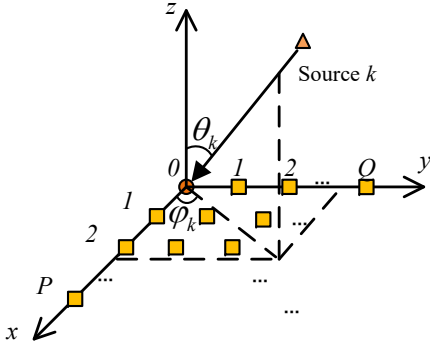


Fig. 2: The UPA model.

As the network environment is generally unchanged for consecutive UL and DL time slots, the UL and DL JCAS can cooperate to enhance both communication and sensing. DL JCAS is capable of sensing both communication users and the dumb scatterers, while UL JCAS can well estimate the user's sensing parameters as the line-of-sight (LoS) path dominates the mmWave JCAS channel. As a consequence, after BS performs a round of DL and UL JCAS, it can merge the results to distinguish between the user and the dumb targets, thus improving the sensing performance. Moreover, the UL and DL CSI estimation results can also be merged to improve the communication performance.

Next, we introduce the JCAS transmit signal model and then demonstrate the JCAS channel models.

B. JCAS Transmit Signal

The UL and DL signals adopt OFDM signals to accommodate the prevalent wireless communication networks. The general OFDM JCAS signal is defined as

$$s^i(t) = \sum_{m=0}^{M_s^i-1} \sum_{n=0}^{N_c^i-1} \sqrt{P_t^i} d_{n,m}^i e^{j2\pi(f_c+n\Delta f^i)t} \text{Rect}\left(\frac{t-mT_s^i}{T_s^i}\right), \quad (1)$$

where $i = U$ or D are for UL and DL JCAS signals, respectively; P_t^i is the transmit power, M_s^i and N_c^i are the numbers of OFDM symbols and subcarriers for each JCAS process, respectively; $d_{n,m}^i$ is the transmit OFDM baseband symbol of the m th OFDM symbol of the n th subcarrier, f_c is the carrier frequency, Δf^i is the subcarrier interval, $T_s^i = \frac{1}{\Delta f^i} + T_g^i$ is the time duration of each OFDM symbol, and T_g^i is the guard interval.

C. UPA Model

Fig. 2 demonstrates the UPA model. The uniform interval between neighboring antenna elements is denoted by d_a . The size of UPA is $P \times Q$. The AoA for receiving or the angle-of-departure (AoD) for transmitting the k th far-field signal is $\mathbf{p}_k = (\varphi_k, \theta_k)^T$, where φ_k is the azimuth angle, and θ_k is the elevation angle. The phase difference between the (p,q) th antenna element and the reference antenna element is

$$a_{p,q}(\mathbf{p}_k) = \exp[-j\frac{2\pi}{\lambda} d_a (p \cos \varphi_k \sin \theta_k + q \sin \varphi_k \sin \theta_k)], \quad (2)$$

where $\lambda = c/f_c$ is the wavelength of the carrier, f_c is the carrier frequency, and c is the speed of light. The steering vector for the array is given by

$$\mathbf{a}(\mathbf{p}_k) = [a_{p,q}(\mathbf{p}_k)]_{|p=0,1,\dots,P-1;q=0,1,\dots,Q-1}, \quad (3)$$

where $\mathbf{a}(\mathbf{p}_k) \in \mathbb{C}^{PQ \times 1}$, and $[v_{p,q}]_{(p,q) \in \mathbf{S1} \times \mathbf{S2}}$ denotes the vector stacked by values $v_{p,q}$ satisfying $p \in \mathbf{S1}$ and $q \in \mathbf{S2}$. The steering matrix for L far-field signals is then given by

$$\mathbf{A} = [\mathbf{a}(\mathbf{p}_1), \mathbf{a}(\mathbf{p}_2), \dots, \mathbf{a}(\mathbf{p}_L)], \quad (4)$$

where $\mathbf{A} \in \mathbb{C}^{PQ \times L}$. Then, we demonstrate the UL and DL JCAS channel models. The sizes of the antenna arrays of the BS and the users are $P_t \times Q_t$ and $P_r \times Q_r$, respectively.

D. JCAS Channel Models

BS estimates the Doppler and range from the UL communication channel using bi-static sensing. Therefore, we name it the UL JCAS channel in this paper. Due to the channel reciprocity, the DL communication channel is the transpose of the UL JCAS channel. The DL echo sensing channel consists of the echo path from UE as a scatterer, and the echo paths from other dumb scatterers, as shown in Fig. 1. Since the signals after multiple reflections are much smaller than those with only one reflection, we only consider echoes directly reflected from scatterers.

Next, we present the expressions for the aforementioned JCAS channels.

1) *UL JCAS Channel Model*: The UL JCAS channel response matrix at the n th subcarrier of the m th OFDM symbol is given by

$$\mathbf{H}_{C,n,m}^U = \sum_{l=0}^{L-1} \begin{bmatrix} b_{C,l} e^{j2\pi(f_{c,d,l})mT_s^U} e^{-j2\pi n \Delta f^U (\tau_{c,l})} \\ \times \mathbf{a}(\mathbf{p}_{RX,l}^U) \mathbf{a}^T(\mathbf{p}_{TX,l}^U) \end{bmatrix}, \quad (5)$$

where $\mathbf{H}_{C,n,m}^U \in \mathbb{C}^{P_t Q_t \times P_r Q_r}$, $l = 0$ is for the channel response of the LoS path, and $l \in \{1, \dots, L-1\}$ is for the paths involved with the l th scatterer; $\mathbf{a}(\mathbf{p}_{RX,l}^U) \in \mathbb{C}^{P_t Q_t \times 1}$ and $\mathbf{a}(\mathbf{p}_{TX,l}^U) \in \mathbb{C}^{P_r Q_r \times 1}$ are the steering vectors for UL receiving and transmission, respectively; $\mathbf{p}_{RX,l}^U$ and $\mathbf{p}_{TX,l}^U$ are the corresponding AoA and AoD, respectively; $f_{c,d,0} = \frac{v_0}{\lambda}$ and $\tau_{c,0} = \frac{r_{0,1}}{c}$ are the Doppler shift and time delay between the user and BS of the LoS path, respectively, with v_0 and $r_{0,1}$ being the corresponding radial relative velocity and the distance, respectively; $f_{c,d,l} = f_{d,l,1} + f_{d,l,2}$ and $\tau_{c,l} = \tau_{c,l,1} + \tau_{c,l,2}$ are the aggregate Doppler shift and time delay of the l th NLoS path, respectively; $f_{d,l,1} = \frac{v_{r,l,1}}{\lambda}$ and $f_{d,l,2} = \frac{v_{r,l,2}}{\lambda}$ are the Doppler shifts between the user and the l th scatterer, and between the l th scatterer and the BS, respectively, with $v_{r,l,1}$ and $v_{r,l,2}$ being the corresponding radial velocities; $\tau_{c,l,1} = \frac{r_{l,1}}{c}$ and $\tau_{c,l,2} = \frac{r_{l,2}}{c}$ are the time delays between the user and the l th scatterer, and between BS and the l th scatterer, respectively, with $r_{l,1}$ and $r_{l,2}$ being the corresponding distances. Moreover, $b_{C,0} = \sqrt{\frac{\lambda^2}{(4\pi r_{0,1})^2}}$ and $b_{C,l} = \sqrt{\frac{\lambda^2}{(4\pi^3 r_{l,1}^2 r_{l,2}^2)}} \beta_{C,l}$ are the attenuation of the LoS and NLoS paths, respectively; $\beta_{C,l}$ is the reflecting factor of the l th scatterer, following $\mathcal{CN}(0, \sigma_{C,\beta,l}^2)$ [14].

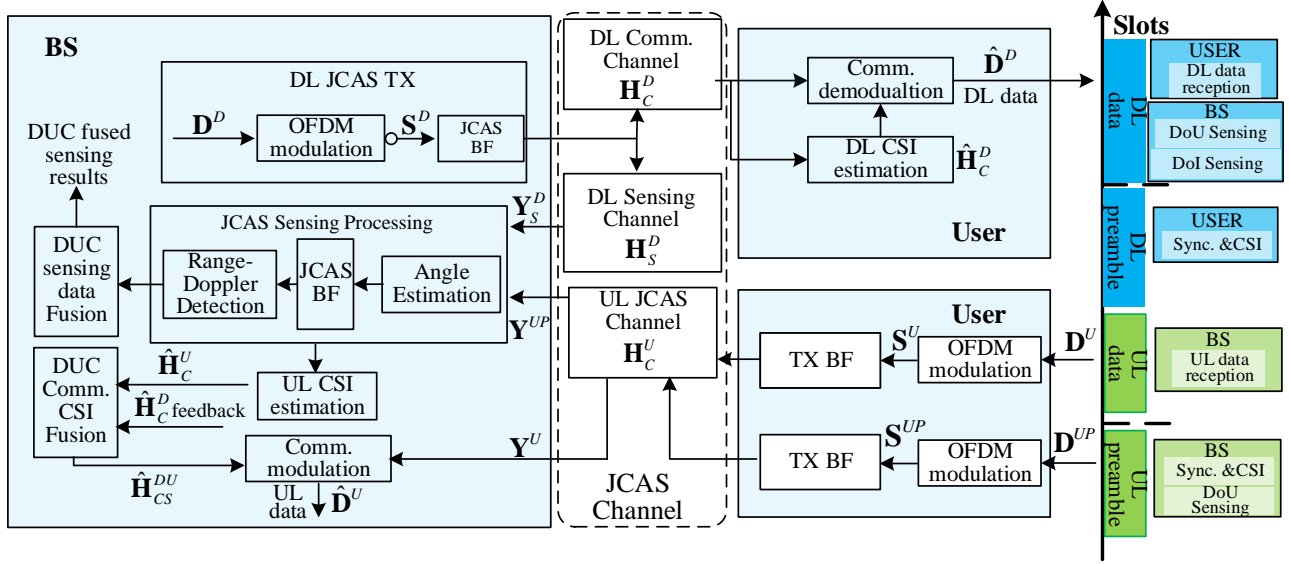


Fig. 3: The illustration of DUC JCAS signal processing.

2) *DL Communication Channel Model*: The DL and UL JCAS adopt the same subcarrier interval and number. Due to the channel reciprocity, the DL communication channel response is the transpose of the UL communication channel response and is given by

$$\mathbf{H}_{C,n,m}^D = \sum_{l=0}^{L-1} \left[b_{C,l} e^{j2\pi(f_{c,d,l})mT_s^D} e^{-j2\pi n\Delta f^D(\tau_{c,l})} \times \mathbf{a}(\mathbf{p}_{RX,l}^D) \mathbf{a}^T(\mathbf{p}_{TX,l}^D) \right], \quad (6)$$

where $\mathbf{H}_{C,n,m}^D \in \mathbb{C}^{P_r Q_r \times P_t Q_t}$, $\mathbf{a}(\mathbf{p}_{TX,l}^D) \in \mathbb{C}^{P_t Q_t \times 1}$ and $\mathbf{a}(\mathbf{p}_{RX,l}^D) \in \mathbb{C}^{P_r Q_r \times 1}$, and $\mathbf{p}_{RX,l}^D = \mathbf{p}_{TX,l}^U$ and $\mathbf{p}_{TX,l}^D = \mathbf{p}_{RX,l}^U$ are the DL communication AoA and AoD, respectively.

3) *DL Echo Sensing Channel Model*: The response of the DL echo sensing channel at the n th subcarrier of the m th OFDM symbol is given by

$$\mathbf{H}_{S,n,m}^D = \sum_{l=0}^{L-1} \left[b_{S,l} e^{j2\pi f_{s,l,1} m T_s^D} e^{-j2\pi n\Delta f^D(\tau_{s,l})} \times \mathbf{a}(\mathbf{p}_{RX,l}^{DS}) \mathbf{a}^T(\mathbf{p}_{TX,l}^D) \right], \quad (7)$$

where $\mathbf{p}_{TX,l}^D$ and $\mathbf{p}_{RX,l}^{DS}$ are the AoD and AoA of the JCAS transmitter and sensing receive array, respectively; $\mathbf{a}(\mathbf{p}_{TX,l}^D) \in \mathbb{C}^{P_t Q_t \times 1}$ and $\mathbf{a}(\mathbf{p}_{RX,l}^{DS}) \in \mathbb{C}^{P_r Q_r \times 1}$ are the corresponding steering vectors as given in (3). Since the mmWave array is typically small, $\mathbf{p}_{RX,l}^{DS} = \mathbf{p}_{TX,l}^D$. Moreover, $f_{s,0,1} = \frac{2v_0}{\lambda}$ and $f_{s,l,1} = \frac{2v_{r,l,2}}{\lambda}$ are the Doppler frequency shifts of the l th echo path, with v_0 and $v_{r,l,2}$ being the corresponding radial relative velocities; $\tau_{s,0} = \frac{2r_{0,1}}{c}$ and $\tau_{s,l} = \frac{2r_{l,2}}{c}$ are the time delays of the l th echo path, with $r_{0,1}$ and $r_{l,2}$ being the corresponding ranges; $b_{S,l} = \sqrt{\frac{\lambda^2}{(4\pi)^3 d_{l,2}^4}} \beta_{S,l}$ with $\beta_{S,l}$ being the reflecting factor of the l th scatterer that follows $\mathcal{CN}(0, \sigma_{\beta_{S,l}}^2)$, according to Swerling model [15].

E. UL and DL Received JCAS Signals

1) *Received Communication Signals*: The received communication signal at the m th OFDM symbol of the n th subcarrier

is

$$\begin{aligned} \mathbf{y}_{C,n,m}^i &= \sqrt{P_t^i} d_{n,m}^i \mathbf{H}_{C,n,m}^i \mathbf{w}_{TX}^i + \mathbf{n}_{t,n,m}^i \\ &= \sqrt{P_t^i} d_{n,m}^i \sum_{l=0}^{L-1} \left[b_{C,l} \chi_{TX,l}^i e^{j2\pi m T_s^i f_{c,d,l}} \times e^{-j2\pi n\Delta f^i \tau_{c,l}} \mathbf{a}(\mathbf{p}_{RX,l}^i) \right] + \mathbf{n}_{t,n,m}^i, \end{aligned} \quad (8)$$

where $i = U$ and D are for UL and DL JCAS signals, respectively; $\mathbf{n}_{t,n,m}^i$ is the combined noise that contains Gaussian noise and possible reflected interferences, and each element of $\mathbf{n}_{t,n,m}^i$ follows $\mathcal{CN}(0, \sigma_N^2)$; $\mathbf{y}_{C,n,m}^U, \mathbf{n}_{t,n,m}^U \in \mathbb{C}^{P_t Q_t \times 1}$, $\mathbf{y}_{C,n,m}^D, \mathbf{n}_{t,n,m}^D \in \mathbb{C}^{P_r Q_r \times 1}$; $d_{n,m}^i$ is the transmit symbol, and P_t^i is the transmit power; \mathbf{w}_{TX}^i is the transmit BF vector, and $\chi_{TX,l}^i = \mathbf{a}^T(\mathbf{p}_{TX,l}^i) \mathbf{w}_{TX}^i$ is the transmit BF gain. We adopt the low-complexity least-square (LS) method to generate \mathbf{w}_{TX}^i , i.e., $\mathbf{w}_{TX}^i = c_0 [\mathbf{a}^T(\tilde{\mathbf{p}}_{TX,l}^i)]^\dagger$ [6], where $[\mathbf{A}]^\dagger$ is the pseudo-inverse matrix of \mathbf{A} , and $c_0 = e^{j2\pi f \phi}$ is a complex value with unit modulus and arbitrary phase. When the transmit beam is well aligned to the user, $\tilde{\mathbf{p}}_{TX,l}^i \approx \mathbf{p}_{TX,l}^i$.

In the ULP and DLP periods, $d_{n,m}^i = \tilde{d}_{n,m}^i$ and $P_t^i = \tilde{P}_t^i$ are the preamble symbols and the corresponding transmit power that are deterministic and known to BS and the user. Without loss of generality, we assume \tilde{P}_t^i is the maximum value of P_t^i . The corresponding received signals for preambles are denoted by $\tilde{\mathbf{y}}_{C,n,m}^i$. In the DLD and ULD periods, $d_{n,m}^i \in \Theta_{QAM}$ is the random data symbol, where Θ_{QAM} is the used quadrature amplitude modulation (QAM) constellation for communication.

2) *Received Echo Sensing Signal*: In the DLD period, the BS can transmit dedicated sensing probe signals to sense the targets in DoI, denoted by \mathbf{p}_S^D . Denote \mathbf{w}_{TX}^{DS} to be the transmit BF vector to illuminate direction \mathbf{p}_S^D . The echo sensing signal received by BS is expressed as

$$\mathbf{y}_{S,n,m}^{DS} = \mathbf{H}_{S,n,m}^D \left(\sqrt{P_t^D} d_{n,m}^{DS} \mathbf{w}_{TX}^{DS} + \sqrt{P_t^{DS}} d_{n,m}^{DS} \mathbf{w}_{TX}^{DS} \right) + \mathbf{n}_{S,n,m}^{DS}, \quad (9)$$

where $\mathbf{y}_{S,n,m}^{DS} \in \mathbb{C}^{P_t Q_t \times 1}$, $d_{n,m}^{DS}$ is the dedicated sensing symbol with unit constant modulus, $d_{n,m}^D$ is the DL communication data symbol; P_t^{DS} and P_t^D are the powers for $d_{n,m}^{DS}$ and $d_{n,m}^D$, respectively; and $P_t^{DS} + P_t^D = \bar{P}_t^D$. Moreover, $\mathbf{n}_{S,n,m}^{DS} \in \mathbb{C}^{P_t Q_t \times 1}$ is the noisy vector that contains Gaussian noise and possible reflected interferences, with each element following $\mathcal{CN}(0, \sigma_N^2)$.

From (7), (8), and (9), we can see that the UL and DL JCAS paths directly formed by the user and BS contain the identical user's range, radial velocity, and AoA. Therefore, the consecutive UL and DL JCAS can conduct independent estimates of several identical sensing parameters, which is the basis for DUC JCAS processing scheme.

III. DUC JCAS SENSING PROCESSING

The DUC JCAS processing scheme is shown in Fig. 3. Specifically, this section demonstrates the unified UL and DL JCAS sensing processing methods, and the JCAS data fusion method will be presented in Section IV. **In this section, we first use a unified MUSIC-based module to estimate the AoA, range and Doppler for the UE in the UL JCAS processing, which are then used for the BF in DL JCAS to suppress the mutual interference between DL sensing and communication. Finally, we show that the DL JCAS processing can use the same MUSIC-based module to estimate the ranges and Doppler frequencies of targets as in the UL JCAS processing.**

A. UL JCAS Processing

In the ULP period, based on (8), the UL CSI estimation at the n th subcarrier of the m th OFDM symbol is obtained with the LS method as [16]

$$\hat{\mathbf{h}}_{C,n,m}^U = \bar{\mathbf{y}}_{C,n,m}^U / (\sqrt{\bar{P}_t^U} \bar{d}_{n,m}^U) \in \mathbb{C}^{P_t Q_t \times 1}, \quad (10)$$

Since N_c^U subcarriers at M_s^U OFDM preamble symbols are used, we can stack all the CSIs to obtain $\hat{\mathbf{H}}_C^U \in \mathbb{C}^{P_t Q_t \times N_c^U M_s^U}$, where the $[(m-1)N_c^U + n]$ th column of $\hat{\mathbf{H}}_C^U$ is $\hat{\mathbf{h}}_{C,n,m}^U$. Denote the UL incident signals of L paths as $\mathbf{s}_{n,m}^U \in \mathbb{C}^{L \times 1}$, where

$$[\mathbf{s}_{n,m}^U]_l = b_{C,l} \chi_{TX,t}^U e^{j2\pi m T_s^U f_{c,d,t}} e^{-j2\pi n \Delta f^U \tau_{c,t}}. \quad (11)$$

Then, $\hat{\mathbf{H}}_C^U$ can be expressed as

$$\hat{\mathbf{H}}_C^U = \mathbf{A}_{U,RX} \mathbf{S}^U + \mathbf{N}_t^U, \quad (12)$$

where $\mathbf{A}_{U,RX} = [\mathbf{a}(\mathbf{p}_{RX,l}^U)]_{l=0,1,\dots,L-1} \in \mathbb{C}^{P_t Q_t \times L}$ is the steering matrix, and the $[(m-1)N_c^U + n]$ th column of \mathbf{N}_t^U is $\mathbf{n}_{t,n,m}^U / (\sqrt{\bar{P}_t^U} \bar{d}_{n,m}^U)$. Moreover, $\mathbf{S}^U \in \mathbb{C}^{L \times N_c^U M_s^U}$ is expressed as

$$\mathbf{S}^U = [\mathbf{s}_{n,m}^U]_{(n,m) \in [0,1,\dots,N_c^U-1] \times [0,1,\dots,M_s^U-1]}. \quad (13)$$

1) *UL JCAS Angle Estimation*: We obtain the AoAs from $\hat{\mathbf{H}}_C^U$ using the refined MUSIC-based estimation method, as referenced to [12]. First, we compute the autocorrelation matrix of \mathbf{Y}_C^U as

$$\mathbf{R}_x^U = [\hat{\mathbf{H}}_C^U (\hat{\mathbf{H}}_C^U)^H] / (M_s^U N_c^U) \in \mathbb{C}^{P_t Q_t \times P_t Q_t}. \quad (14)$$

Applying eigenvalue decomposition to \mathbf{R}_x^U , we obtain

$$[\mathbf{U}_x^U, \boldsymbol{\Sigma}_x^U] = \text{eig}(\mathbf{R}_x^U), \quad (15)$$

where $\text{eig}(\mathbf{M})$ represents the eigenvalue decomposition of \mathbf{M} , $\boldsymbol{\Sigma}_x^U$ is the real-value eigenvalue diagonal matrix in descending order, and \mathbf{U}_x^U is the orthogonal eigen matrix. The number of incident signals is denoted by N_x^U . The noise subspace of \mathbf{R}_x^U is $\mathbf{U}_N^U = [\mathbf{U}_x^U]_{:,N_x^U+1:P_t Q_t}$, and then we formulate the angle spectrum function as [17]

$$f_a^U(\mathbf{p}) = \mathbf{a}^H(\mathbf{p}) \mathbf{U}_N^U (\mathbf{U}_N^U)^H \mathbf{a}(\mathbf{p}), \quad (16)$$

where $\mathbf{a}(\mathbf{p})$ is given in (3). The angle spectrum is further obtained as [17]

$$S_a^U(\mathbf{p}) = [\mathbf{a}^H(\mathbf{p}) \mathbf{U}_N^U (\mathbf{U}_N^U)^H \mathbf{a}(\mathbf{p})]^{-1}. \quad (17)$$

The minimum points of $f_a^U(\mathbf{p})$, i.e., the maximum points of $S_a^U(\mathbf{p})$ are the estimated AoAs. We then use a 2D two-step Newton descent method in [12] to derive the minimum points of $f_a^U(\mathbf{p})$, which is demonstrated in **Algorithm 1**. The initial points for Newton descent iteration are given by a coarse-granularity grid search [10].

To identify the minimum of $f_a^U(\mathbf{p})$, we substitute $f(\mathbf{p})$, $\mathbf{H}_p(\mathbf{p})$, and $\nabla_p f(\mathbf{p})$ in **Algorithm 1** with (16), Hessian matrix and the gradient vector of $f_a^U(\mathbf{p})$, respectively. Note that **Algorithm 1** can also be used in the one-dimensional (1D) parameter estimation by treating the second parameter to be a constant value.

By applying **Algorithm 1**, we estimate the AoAs denoted by $\Theta^U = \{\hat{\mathbf{p}}_k^U\}_{k \in \{0,1,\dots,N_x^U-1\}}$. Moreover, Θ^U is sorted in the descending order by the value of $S_a^U(\hat{\mathbf{p}}_k^U)$. **Typically, $\hat{\mathbf{p}}_0^U$ is the estimated user's AoA because the LoS path dominates the UL JCAS channel.**

The BF matrix to receive the incident signals can be obtained by solving the following optimization problem:

$$\mathbf{W}_{RX}^U = \arg \min_{\mathbf{W}} \|\mathbf{W}^H \mathbf{A}_{U,RX} \mathbf{S}^U - \mathbf{S}^U\|_2^2, \quad (18)$$

where the m th column of \mathbf{W}_{RX}^U is the BF vector that receives the signal from the m th direction in Θ^U . Since the problem is convex, we have

$$\mathbf{W}_{RX}^U = [\mathbf{A}_{U,RX} (\mathbf{A}_{U,RX})^H]^{-1} \mathbf{A}_{U,RX}. \quad (19)$$

For the estimated steering matrix, i.e., $\tilde{\mathbf{A}}_{U,RX} = [\mathbf{a}(\hat{\mathbf{p}}_k^U)]_{k=0,1,\dots,N_x^U-1}$, the received BF matrix is expressed as

$$\tilde{\mathbf{W}}_{RX}^U = [\tilde{\mathbf{A}}_{U,RX} (\tilde{\mathbf{A}}_{U,RX})^H]^{-1} \tilde{\mathbf{A}}_{U,RX}. \quad (20)$$

Then, we normalize each column of $\tilde{\mathbf{W}}_{RX}^U$ to obtain $\bar{\mathbf{W}}_{RX}^U$. Since the LoS path generally has dominant power in mmWave systems, we use the first column of $\bar{\mathbf{W}}_{RX}^U$, denoted by $\mathbf{w}_{RX}^U = [\bar{\mathbf{W}}_{RX}^U]_{:,1}$, to constructively combine the LoS path's signals.

Then, the UL CSI obtained by BS is

$$\hat{\mathbf{h}}_{CS}^U = (\mathbf{w}_{RX}^U)^H \hat{\mathbf{H}}_C^U, \quad (21)$$

where $\hat{\mathbf{h}}_{CS}^U \in \mathbb{C}^{1 \times N_c^U M_s^U}$ also includes the LoS path's sensing parameters.

Algorithm 1: 2D two-step Newton descent minimum searching method [12]

Input: The range of φ : Φ_φ ; the range of θ : Φ_θ ; the number of initial grid points: N_i ; the maximum iteration round ind_{max} ; the MUSIC spectrum function: $f(\mathbf{p})$.

Output: Estimation results: $\Theta = \{\hat{\mathbf{p}}_k\}_{k \in \{0, \dots, N_s - 1\}}$.

Initialize:

1) Φ_φ and Φ_θ are both divided evenly into $N_i - 1$ pieces by N_i grid points to generate a meshgrid $\hat{\Phi}_\varphi \times \hat{\Phi}_\theta$.

2) Set a null space Θ .

Process:

Step 1: foreach $\mathbf{p}_{i,j} \in \hat{\Phi}_\varphi \times \hat{\Phi}_\theta$ do

Calculate the spatial spectrum as \mathbf{S} , where
 $[\mathbf{S}]_{i,j} = [f(\mathbf{p}_{i,j})]^{-1}$.

end

Step 2: Search the maximal values of \mathbf{S} to form the set Θ_d .

Step 3: Derive the Hessian matrix and the gradient vector of $f(\mathbf{p})$ as $\mathbf{H}_\mathbf{p}(\mathbf{p})$ and $\nabla_\mathbf{p}f(\mathbf{p})$, respectively.

Step 4: foreach $\mathbf{p}_{i,j} \in \Theta_d$ do

$k=1$;
 $\mathbf{p}^{(0)} = \mathbf{p}_{i,j}$;
 $\mathbf{p}^{(k)} = \mathbf{p}^{(k-1)} - [\mathbf{H}_\mathbf{p}(\mathbf{p}^{(k-1)})]^{-1} \nabla_\mathbf{p}f(\mathbf{p}^{(k-1)})$;
while $\|\mathbf{p}^{(k)} - \mathbf{p}^{(k-1)}\| > \varepsilon$ **and** $k \leq ind_{max}$ **do**
 $\mathbf{p}^{(k)} = \mathbf{p}^{(k-1)} - [\mathbf{H}_\mathbf{p}(\mathbf{p}^{(k-1)})]^{-1} \nabla_\mathbf{p}f(\mathbf{p}^{(k-1)})$;
end
 $\mathbf{p}^{(k)}$ is put into output set Θ ;

end

2) *UL JCAS Range-Doppler Estimation:* Reshape $\hat{\mathbf{H}}_{CS}^U$ to a $N_c^U \times M_s^U$ matrix, denoted by $\hat{\mathbf{H}}_{CS}^U$, then combine (11), (12), (13) and (21). We can obtain the (n, m) th element of $\hat{\mathbf{H}}_{CS}^U$ as

$$\begin{aligned} \hat{h}_{CS,n,m}^U &= h_{CS,n,m}^U + w_{t,n,m}^U \\ &= \sum_{l=0}^{L-1} \left[b_{C,l} e^{j2\pi n T_s^U f_{c,d,l}} e^{-j2\pi n \Delta f^U \tau_{c,l}} \right] + w_{t,n,m}^U, \end{aligned} \quad (22)$$

where $w_{t,n,m}^U = (\mathbf{w}_{RX}^U)^H \mathbf{n}_{t,n,m}^U / (\sqrt{P_t^U} \bar{d}_{n,m}^U)$ is the transformed noise, $h_{CS,n,m}^U = (\mathbf{w}_{RX}^U)^H \mathbf{H}_{C,n,m}^U \mathbf{w}_{TX}^U$ is the actual communication CSI, and $\varpi_{RX,l}^U = (\mathbf{w}_{RX}^U)^H \mathbf{a}(\mathbf{p}_{RX,l}^U)$ is the gain at the l th AoA. Since \mathbf{w}_{RX}^U points at the LoS path, $\varpi_{RX,0}^U$ is much larger than $\varpi_{RX,l}^U$ ($l \neq 0$).

Notice that $\hat{h}_{CS,n,m}^U$ contains independent complex exponential functions for range and Doppler, i.e., $e^{j2\pi n T_s^U f_{c,d,l}}$ and $e^{-j2\pi n \Delta f^U \tau_{c,l}}$. Here, we define the range and Doppler steering vectors, respectively, as

$$\mathbf{a}_r(r; \Delta f, N_c) = [e^{-j2\pi n \Delta f^U \tau_c^r}]_{n=0,1,\dots,N_c-1}, \quad (23)$$

$$\mathbf{a}_f(f; T_s, M_s) = [e^{j2\pi m T_s^U f}]_{m=0,1,\dots,M_s-1}. \quad (24)$$

Then, the UL range and Doppler steering matrices are defined as

$$\mathbf{A}_r^U = [\mathbf{a}_r(r_l; \Delta f^U, N_c^U)]_{l=0,1,\dots,L-1} \in \mathbb{C}^{N_c^U \times L}, \quad (25)$$

$$\mathbf{A}_f^U = [\mathbf{a}_f(f_{c,d,l}; T_s^U, M_s^U)]_{l=0,1,\dots,L-1} \in \mathbb{C}^{M_s^U \times L}, \quad (26)$$

where $r_l = \tau_{c,l} \times c$.

According to (22), $\hat{\mathbf{H}}_{CS}^U$ can be written in matrix form as

$$\hat{\mathbf{H}}_{CS}^U = \mathbf{A}_r^U \mathbf{S}_S^U (\mathbf{A}_f^U)^T + \mathbf{W}_{tr}^U, \quad (27)$$

where $\mathbf{S}_S^U = \text{diag}([\sqrt{P_t^U} b_{C,l} \varpi_{RX,l}^U \chi_{TX,l}^U]_{l=0,\dots,L-1})$ is irrelevant to \mathbf{A}_r^U and \mathbf{A}_f^U , and $[\mathbf{W}_{tr}^U]_{n,m} = w_{t,n,m}^U$. We use the **Theorem 1** in [12], to estimate the range and Doppler.

Theorem 1. The range and Doppler steering matrices are $\mathbf{A}_r = [\mathbf{a}_r(r_l; \Delta f, N_c)]_{l=0,1,\dots,L-1}$ and $\mathbf{A}_f = [\mathbf{a}_f(f_l; T, M_s)]_{l=0,1,\dots,L-1}$. If $\hat{\mathbf{H}} = \mathbf{A}_r \mathbf{S}_s (\mathbf{A}_f)^T + \mathbf{W} \in \mathbb{C}^{N_c \times M_s}$, where $\mathbf{S}_s = \text{diag}([a_l]_{l=0,\dots,L-1})$, a_l is a complex value irrelevant to \mathbf{A}_r and \mathbf{A}_f , and \mathbf{W} is zero-mean Gaussian noise matrix. Let the noise subspaces of $\hat{\mathbf{H}}$ and $\hat{\mathbf{H}}^T$ be $\mathbf{U}_{x,rN}$ and $\mathbf{U}_{x,fN}$, respectively. Then, the minimal values of $\|\mathbf{U}_{x,rN}^H \mathbf{a}_r(r)\|_2^2$ and $\|\mathbf{U}_{x,fN}^H \mathbf{a}_f(f)\|_2^2$ are $r = r_l$ and $f = f_l$, respectively [12].

Proof. The proof is provided in the **Appendix C** in [12]. \square

Based on **Theorem 1**, following the same approach as taken in (14)-(17), we can obtain the range and Doppler spectra. From the spectra, we use the steps 3-4 in **Algorithm 1** to find the peaks that are the estimates of ranges and Doppler frequencies. We first derive the correlation matrices of $\hat{\mathbf{H}}_{CS}^U$ and $(\hat{\mathbf{H}}_{CS}^U)^T$, respectively, as

$$\mathbf{R}_{x,r}^U = \frac{1}{M_s^U} \hat{\mathbf{H}}_{CS}^U (\hat{\mathbf{H}}_{CS}^U)^H \in \mathbb{C}^{N_c^U \times N_c^U}, \quad (28)$$

$$\mathbf{R}_{x,f}^U = \frac{1}{N_c^U} (\hat{\mathbf{H}}_{CS}^U)^T (\hat{\mathbf{H}}_{CS}^U)^* \in \mathbb{C}^{M_s^U \times M_s^U}. \quad (29)$$

By applying eigenvalue decomposition to $\mathbf{R}_{x,r}^U$ and $\mathbf{R}_{x,f}^U$, we obtain

$$\begin{aligned} [\mathbf{U}_{x,r}^U, \mathbf{\Sigma}_{x,r}^U] &= \text{eig}(\mathbf{R}_{x,r}^U), \\ [\mathbf{U}_{x,f}^U, \mathbf{\Sigma}_{x,f}^U] &= \text{eig}(\mathbf{R}_{x,f}^U), \end{aligned} \quad (30)$$

respectively, where $\mathbf{\Sigma}_{x,r}^U$ and $\mathbf{\Sigma}_{x,f}^U$ are the eigenvalue diagonal matrices, $\mathbf{U}_{x,r}^U$ and $\mathbf{U}_{x,f}^U$ are the corresponding eigen matrices, respectively. The number of targets is denoted by $N_{x,s}^U$. The noise subspaces of $\mathbf{R}_{x,r}^U$ and $\mathbf{R}_{x,f}^U$ are $\mathbf{U}_{x,rN}^U = [\mathbf{U}_{x,r}^U]_{:,N_{x,s}^U+1:N_c^U}$ and $\mathbf{U}_{x,fN}^U = [\mathbf{U}_{x,f}^U]_{:,N_{x,s}^U+1:M_s^U}$, respectively. The range and Doppler spectrum functions are, respectively, given by

$$f_r^U(r) = \mathbf{a}_r^U(r)^H \mathbf{U}_{x,rN}^U (\mathbf{U}_{x,rN}^U)^H \mathbf{a}_r^U(r), \quad (31)$$

$$f_f^U(f) = \mathbf{a}_f^U(f)^H \mathbf{U}_{x,fN}^U (\mathbf{U}_{x,fN}^U)^H \mathbf{a}_f^U(f). \quad (32)$$

where $\mathbf{a}_r^U(r) = \mathbf{a}_r(r; \Delta f^U, N_c^U)$, and $\mathbf{a}_f^U(f) = \mathbf{a}_f(f; T_s^U, M_s^U)$. Furthermore, the range and Doppler spectra are, respectively, given by

$$S_r^U(r) = [\mathbf{a}_r^U(r)^H \mathbf{U}_{x,rN}^U (\mathbf{U}_{x,rN}^U)^H \mathbf{a}_r^U(r)]^{-1}, \quad (33)$$

$$S_f^U(f) = [\mathbf{a}_f^U(f)^H \mathbf{U}_{x,fN}^U (\mathbf{U}_{x,fN}^U)^H \mathbf{a}_f^U(f)]^{-1}. \quad (34)$$

According to **Theorem 1**, the minimal points of $f_r^U(r)$ or $f_f^U(f)$, i.e., the maximal points of $S_r^U(r)$ or $S_f^U(f)$ are the range and Doppler estimation results. **Algorithm 1** can be used

to identify the above minimal values by reducing the second parameter, θ , in **Algorithm 1** to be a **redundant** constant [12]. Note that $f(\mathbf{p})$, $\nabla_{\mathbf{p}} f(\mathbf{p})$ and $\mathbf{H}_{\mathbf{p}}(f)$ in **Algorithm 1** are replaced by (31), $\frac{\partial f_r^U(r)}{\partial r}$, and $\frac{\partial^2 f_r^U(r)}{\partial^2 r}$ for range estimation, and replaced by (32), $\frac{\partial f_f^U(f)}{\partial f}$, and $\frac{\partial^2 f_f^U(f)}{\partial^2 f}$ for Doppler estimation, respectively.

The estimated range and Doppler sets are denoted by $\Theta_r^U = [\hat{r}_{k1}^U]_{k1=0, \dots, N_{x,s}^U-1}$ and $\Theta_f^U = [\hat{f}_{k2}^U]_{k2=0, \dots, N_{x,s}^U-1}$, respectively. Then, we provide the range-Doppler matching method to match the decoupled range and Doppler estimation results.

3) *Range-Doppler Matching Method*: The range and Doppler results are matched according to **Theorem 2**.

Theorem 2. If $\hat{\mathbf{H}} = \mathbf{A}_r \mathbf{S} (\mathbf{A}_f)^T + \mathbf{W}$, where \mathbf{W} is a Gaussian noise matrix, \mathbf{S} is a diagonal matrix irrelevant to \mathbf{A}_r and \mathbf{A}_f , $\mathbf{A}_r = [\mathbf{a}_r(r_l; \Delta f, N_c)]_{l=0,1, \dots, L-1}$, and $\mathbf{A}_f = [\mathbf{a}_f(f_l; T_s, M_s)]_{l=0,1, \dots, L-1}$, then only the range-Doppler pair of the same target, denoted by $(r = r_l, f = f_l)$, can achieve the maximal points of $\|[\mathbf{a}_r(r)]^H \mathbf{A}_r \mathbf{S} (\mathbf{A}_f)^T [\mathbf{a}_f(f)]^*\|_2^2$.

Proof. The proof is provided in **Appendix A**. \square

According to **Theorem 2**, we define the range-Doppler matching matrix for UL JCAS as

$$\mathbf{M}_{r,f}^U = \|[\tilde{\mathbf{A}}_r^U]^H \hat{\mathbf{H}}_{CS}^U [\tilde{\mathbf{A}}_f^U]^*\|_2^2 \in \mathbb{C}^{N_{x,s}^U \times N_{x,s}^U}, \quad (35)$$

where $\tilde{\mathbf{A}}_r^U = [\mathbf{a}_r(r; \Delta f^U, N_c^U)]_{r \in \Phi_r^U}$ and $\tilde{\mathbf{A}}_f^U = [\mathbf{a}_f(f; T_s^U, M_s^U)]_{f \in \Phi_f^U}$ are the estimated range and Doppler steering matrices for UL JCAS, respectively. The maximum of the n th row of $\mathbf{M}_{r,f}^U$, e.g., $[\mathbf{M}_{r,f}^U]_{n,m_n}$, indicates the n th value of Φ_r^U matches the m_n th value of Φ_f^U .

B. DLP CSI Estimation

In the DLP period, the user receives the preamble signals from BS using receive BF vector, denoted by \mathbf{w}_{RX}^D . The received preamble signal is given by

$$\begin{aligned} \bar{y}_{C,n,m}^D &= (\mathbf{w}_{RX}^D)^H \bar{y}_{C,n,m}^D \\ &= \sqrt{P_t^D} \bar{d}_{n,m}^D \sum_{l=0}^{L-1} \begin{bmatrix} b_{C,l} e^{j2\pi m T_s^D f_{c,d,l}} \\ \times e^{-j2\pi n \Delta f^D \tau_{c,l}} \\ \times \chi_{TX,l}^D \varpi_{RX,l}^D \end{bmatrix} + n_{t,n,m}^D \end{aligned} \quad (36)$$

where $\bar{y}_{C,n,m}^D$ is given in (8), and $n_{t,n,m}^D = (\mathbf{w}_{RX}^D)^H \mathbf{n}_{t,n,m}^D$. Moreover, due to channel reciprocity, we have $\mathbf{w}_{RX}^D = \mathbf{w}_{TX}^U$ and $\mathbf{w}_{TX}^D = \mathbf{w}_{RX}^U$. Therefore, $\varpi_{RX,l}^D = \chi_{TX,l}^U$ and $\chi_{TX,l}^D = \varpi_{RX,l}^U$. According to [16], the DL communication CSI obtained with the LS method is

$$\hat{h}_{CS,n,m}^D = \frac{\bar{y}_{C,n,m}^D}{\sqrt{P_t^D} \bar{d}_{n,m}^D} = h_{CS,n,m}^D + w_{t,n,m}^D, \quad (37)$$

where $h_{CS,n,m}^D = h_{CS,n,m}^U$ is due to the channel reciprocity, and $w_{t,n,m}^D = n_{t,n,m}^D / (\sqrt{P_t^D} \bar{d}_{n,m}^D)$ is the transformed noise.

C. DLD Period Mono-static JCAS Processing

In this subsection, we first present the received DL data and echo signals after BF, then propose the DLD JCAS BF and sensing schemes.

1) *Received DL Data and Echo Signals*: In the DLD period, BS transmits data signals to the user using the communication link formed in the DLP period. Except for data communication, BS also transmits dedicated sensing beam to DoI, \mathbf{p}_S^D , with BF vector, \mathbf{w}_{TX}^{DS} . The value of \mathbf{w}_{TX}^{DS} should be optimized to minimize the interference to DL communication.

The DL data signal received by the user is expressed as

$$\begin{aligned} y_{C,n,m}^D &= \mathbf{h}_{C,n,m}^D \begin{bmatrix} d_{n,m}^D \sqrt{P_t^D} \mathbf{w}_{TX}^D \\ + d_{n,m}^{DS} \sqrt{P_t^{DS}} \mathbf{w}_{TX}^{DS} \end{bmatrix} + w_{C,n,m}^D \\ &= d_{n,m}^D \sqrt{P_t^D} h_{CS,n,m}^D + d_{n,m}^{DS} \sqrt{P_t^{DS}} h_{CS,n,m}^D \mathbf{w}_{TX}^{DS} + w_{C,n,m}^D, \end{aligned} \quad (38)$$

where $\mathbf{h}_{C,n,m}^D = (\mathbf{w}_{RX}^D)^H \mathbf{H}_{C,n,m}^D \in \mathbb{C}^{1 \times P_t Q_t}$, $w_{C,n,m}^D = (\mathbf{w}_{RX}^D)^H \mathbf{n}_{t,n,m}^D$, and $d_{n,m}^{DS}$ and P_t^{DS} are the transmit probe symbol and power, respectively. Note that the second term in (38) is the interference to DL communication.

In this process, \mathbf{w}_{TX}^{DS} should be interference-free to DL communication. Therefore, \mathbf{w}_{TX}^{DS} is in the nullspace of $\mathbf{h}_{C,n,m}^D$. Due to the channel reciprocity, we can use $(\hat{\mathbf{h}}_{C,n,m}^U)^T$ to replace $\mathbf{h}_{C,n,m}^D$. By deriving the singular value decomposition of $(\hat{\mathbf{h}}_{C,n,m}^U)^T$, the right singular matrix is obtained as $\mathbf{V}_{C,n,m}^D$, and the nullspace basis can be derived as

$$\mathbf{V}_{C,n,m}^{DN} = [\mathbf{V}_{C,n,m}^D]_{:,2:P_t Q_t} \in \mathbb{C}^{P_t Q_t \times (P_t Q_t - 1)}. \quad (39)$$

Then, \mathbf{w}_{TX}^{DS} should be the linear transform of $\mathbf{V}_{C,n,m}^{DN}$ to guarantee no interference to the DL communication, i.e.,

$$\mathbf{w}_{TX}^{DS} = \mathbf{V}_{C,n,m}^{DN} \mathbf{m}_1, \quad (40)$$

where $\mathbf{m}_1 \in \mathbb{C}^{(P_t Q_t - 1) \times 1}$ and will be finally determined in the following subsection.

On the other hand, to receive both the echo signals of the DL communication signal and those of the dedicated sensing signal, BS generates a BF matrix, $\mathbf{W}_{RX}^{DS} = [\mathbf{w}_{n,m}^D, \mathbf{w}_{n,m}^{DS}] \in \mathbb{C}^{P_t Q_t \times 2}$, to distinguish the echo signals from these two directions. The echo signals received at BS in the n th sub-carrier of the m th OFDM symbol is expressed as $\mathbf{r}_{S,n,m}^{DS} = (\mathbf{W}_{RX}^{DS})^H \mathbf{y}_{S,n,m}^{DS}$. Combining (9), we express the sensing echo signal as

$$\mathbf{r}_{S,n,m}^{DS} = (\mathbf{W}_{RX}^{DS})^H \mathbf{H}_{S,n,m}^D \begin{pmatrix} \sqrt{P_t^D} d_{n,m}^D \mathbf{w}_{TX}^D \\ + \sqrt{P_t^{DS}} d_{n,m}^{DS} \mathbf{w}_{TX}^{DS} \end{pmatrix} + \bar{\mathbf{n}}_{S,n,m}^{DS}, \quad (41)$$

where $\bar{\mathbf{n}}_{S,n,m}^{DS} = (\mathbf{W}_{RX}^{DS})^H \mathbf{n}_{S,n,m}^D$. Note that \mathbf{w}_{TX}^D generates the JCAS beam pointed at the estimated user's direction, $\hat{\mathbf{p}}_0^U$; \mathbf{w}_{TX}^{DS} generates the beam pointed at DoI, \mathbf{p}_S^D ; and \mathbf{W}_{RX}^{DS} is aimed to distinguish the echo signals from these two directions.

2) *DLD JCAS BF Method*: Since $\mathbf{H}_{S,n,m}^D$ is unknown before transmitting JCAS signals, we have to use reference channel responses to generate \mathbf{w}_{TX}^{DS} and \mathbf{W}_{RX}^{DS} . The reference channel responses can be generated via **Theorem 3** based on the estimated UE's AoA and range.

Theorem 3. The actual mono-static echo sensing channel, denoted by \mathbf{H}_{SU} , has the same form as (7), and is composed of K scatterers with direction $\Theta = \{\mathbf{p}_{S,k}\}_{k=0, \dots, K-1}$. Its

DoI is \mathbf{p}_S , and the reference channel response can be defined as

$$\mathbf{H}_{RS} = \sqrt{\lambda^2 / \left[(4\pi)^3 (r_E)^4 \right]} \mathbf{a}(\mathbf{p}_S) \mathbf{a}^T(\mathbf{p}_S), \quad (42)$$

where r_E is the expected range of the target. The receive and transmit BF vectors generated from \mathbf{H}_{RS} , denoted, respectively, by \mathbf{w}_{RX} and \mathbf{w}_{TX} , have the following properties: The value set $\{\mathbf{w}_{RX}, \mathbf{w}_{TX}\} = \{\mathbf{w}_{RX}^0, \mathbf{w}_{TX}^0\}$ that satisfies $\|(\mathbf{w}_{RX}^0)^H \mathbf{H}_{RS} \mathbf{w}_{TX}^0\|_2^2 = 0$ can make $\|(\mathbf{w}_{RX}^0)^H \mathbf{H}_{SU} \mathbf{w}_{TX}^0\|_2^2 \approx 0$; the value set $\{\mathbf{w}_{RX}, \mathbf{w}_{TX}\} = \{\mathbf{w}_{RX}^{max}, \mathbf{w}_{TX}^{max}\}$ that maximizes $\|(\mathbf{w}_{RX})^H \mathbf{H}_{RS} \mathbf{w}_{TX}\|_2^2$ can also maximize $\|(\mathbf{w}_{RX})^H \mathbf{H}_{SU} \mathbf{w}_{TX}\|_2^2$.

Proof. The proof is provided in **Appendix B**. \square

According to **Theorem 3**, we can define the reference channel matrix for generating $\mathbf{w}_{n,m}^{DS}$ and \mathbf{w}_{TX}^{DS} as

$$\mathbf{H}_{RS,n,m}^D = \sqrt{\lambda^2 / \left[(4\pi)^3 (r_E)^4 \right]} \mathbf{a}(\mathbf{p}_S^D) \mathbf{a}^T(\mathbf{p}_S^D), \quad (43)$$

where r_E is the expected range of the target. Similarly, the reference channel matrix for generating $\mathbf{w}_{n,m}^D$ is defined as

$$\mathbf{H}_{IS,n,m}^D = \sqrt{\lambda^2 / \left[(4\pi)^3 (\hat{r}_0^U)^4 \right]} \mathbf{a}(\hat{\mathbf{p}}_0^U) \mathbf{a}^T(\hat{\mathbf{p}}_0^U), \quad (44)$$

where $\hat{\mathbf{p}}_0^U$ and \hat{r}_0^U are the estimated direction and range of the user estimated in Section III-A. Here, we set $r_E = \hat{r}_0^U$ to balance the propagation loss of two echo signals. The reference received signal can be expressed with $\mathbf{H}_{RS,n,m}^D$ and $\mathbf{H}_{IS,n,m}^D$, and is given by

$$\mathbf{r}_{RS,n,m}^{DS} = (\mathbf{W}_{RX}^{DS})^H \begin{pmatrix} \mathbf{H}_{IS,n,m}^D \sqrt{P_t^D} d_{n,m}^D \mathbf{w}_{TX}^D + \\ \mathbf{H}_{RS,n,m}^D \sqrt{P_t^{DS}} d_{n,m}^{DS} \mathbf{w}_{TX}^{DS} \end{pmatrix}. \quad (45)$$

Since $\mathbf{w}_{TX}^{DS} = \mathbf{V}_{C,n,m}^{DN} \mathbf{m}_1$ and $\mathbf{W}_{RX}^{DS} = [\mathbf{w}_{n,m}^D, \mathbf{w}_{n,m}^{DS}]$ are designed by maximizing the received signals while eliminating the interference, the criterion to generate $\mathbf{w}_{n,m}^{DS}$ and $\mathbf{W}_{RX}^{DS} = [\mathbf{w}_{n,m}^D, \mathbf{w}_{n,m}^{DS}]$ can be, respectively, given by

$$\begin{aligned} \max_{\mathbf{w}_{n,m}^D} & \|(\mathbf{w}_{n,m}^D)^H \mathbf{H}_{IS,n,m}^D \mathbf{w}_{TX}^D\|_2^2 \\ \text{s.t.} & (\mathbf{w}_{n,m}^D)^H \mathbf{H}_{RS,n,m}^D = \mathbf{0} \\ & \|\mathbf{w}_{n,m}^D\|_2^2 = 1 \end{aligned}, \quad (46)$$

$$\begin{aligned} \max_{\mathbf{w}_{n,m}^{DS}, \mathbf{m}_1} & \|(\mathbf{w}_{n,m}^{DS})^H \mathbf{H}_{RS,n,m}^D \mathbf{V}_{C,n,m}^{DN} \mathbf{m}_1\|_2^2 \\ \text{s.t.} & (\mathbf{w}_{n,m}^{DS})^H \mathbf{H}_{IS,n,m}^D = \mathbf{0} \\ & \|\mathbf{w}_{n,m}^{DS}\|_2^2 = \|\mathbf{m}_1\|_2^2 = 1 \end{aligned}. \quad (47)$$

The derivation of $\mathbf{w}_{n,m}^D$, $\mathbf{w}_{n,m}^{DS}$, and \mathbf{w}_{TX}^{DS} is provided in **Appendix C**. The final solutions to them are

$$\begin{aligned} \mathbf{w}_{n,m}^D &= \mathbf{U}_{RS,n,m}^{DN} [\mathbf{U}_{IS}^D]_{:,1}, \\ \mathbf{w}_{n,m}^{DS} &= \mathbf{U}_{IS,n,m}^{DN} [\mathbf{U}_{RS}^D]_{:,1}, \\ \mathbf{w}_{TX}^{DS} &= \mathbf{V}_{C,n,m}^{DN} [\mathbf{V}_{RS}^D]_{:,1}, \end{aligned} \quad (48)$$

where $\mathbf{U}_{RS,n,m}^{DN}$ and $\mathbf{U}_{IS,n,m}^{DN}$ are the left singular matrices of $\mathbf{H}_{RS,n,m}^D$ and $\mathbf{H}_{IS,n,m}^D$, respectively; \mathbf{U}_{IS}^D is the left singular matrix of $(\mathbf{U}_{RS,n,m}^{DN})^H \mathbf{H}_{IS,n,m}^D \mathbf{w}_{TX}^D$, and \mathbf{U}_{RS}^D

and \mathbf{V}_{RS}^D are the left and right singular matrices of $(\mathbf{U}_{IS,n,m}^{DN})^H \mathbf{H}_{RS,n,m}^D \mathbf{V}_{C,n,m}^{DN}$.

Substituting (48) into (41) and (38), the received DL communication signals and echo signals are formed completely. Subsequently, we present the DLD period sensing signal processing methods.

3) *DLD Period Sensing Signal Processing*: Since (48) are solutions to the problems (46) and (47), according to **Theorem 3**, $[\mathbf{r}_{S,n,m}^{DS}]_1$ and $[\mathbf{r}_{S,n,m}^{DS}]_2$ are the echo signals from directions, $\hat{\mathbf{p}}_0^D$ and \mathbf{p}_S^D , respectively. In order to obtain the ranges and Doppler frequencies of targets from $\mathbf{r}_{S,n,m}^{DS}$, the transmit symbols are removed first, and we obtain $\hat{h}_{S1,n,m}^{DS} = [\mathbf{r}_{S,n,m}^{DS}]_1 / d_{n,m}^D$ and $\hat{h}_{S2,n,m}^{DS} = [\mathbf{r}_{S,n,m}^{DS}]_2 / d_{n,m}^{DS}$. According to (41), we have

$$\begin{aligned} \hat{h}_{S1,n,m}^{DS} &= \sum_{l=0}^{L-1} \left[b_{S,l} \chi_{RX,l}^D \chi_{TX,l}^D \sqrt{P_t^D} \right. \\ & \quad \left. \times e^{j2\pi f_{s,l,1} T_s^D} e^{-j2\pi n \Delta f^D \tau_{s,l}} \right] + N_{S1,n,m}^{DS}, \\ \hat{h}_{S2,n,m}^{DS} &= \sum_{k=0}^{K-1} \left[b_{S,k} \chi_{RX,k}^{DS} \chi_{TX,k}^{DS} \sqrt{P_t^{DS}} \right. \\ & \quad \left. \times e^{j2\pi m T_s^D f_{d,k}^{SU}} e^{-j2\pi n \Delta f^D \frac{2r_k^{RS}}{c}} \right] + N_{S2,n,m}^{DS}, \end{aligned} \quad (49)$$

respectively, where K is the number of targets in DoI, $f_{d,k}^{SU}$ and r_k^{RS} are the Doppler and range of the k th target in DoI; $\chi_{RX,l}^D = (\mathbf{w}_{n,m}^D)^H \mathbf{a}(\mathbf{p}_{RX,l}^D)$, $\chi_{TX,l}^D = \mathbf{a}^T(\mathbf{p}_{TX,l}^D) \mathbf{w}_{TX}^D$, $\chi_{RX,k}^{DS} = (\mathbf{w}_{n,m}^{DS})^H \mathbf{a}(\mathbf{p}_{RX,k}^D)$, and $\chi_{TX,k}^{DS} = \mathbf{a}^T(\mathbf{p}_{TX,k}^D) \mathbf{w}_{TX}^{DS}$ are the BF gains. Moreover, $N_{S1,n,m}^{DS} = (\mathbf{w}_{n,m}^D)^H (\mathbf{n}_{S,n,m}^{DS}) / d_{n,m}^D$ and $N_{S2,n,m}^{DS} = (\mathbf{w}_{n,m}^{DS})^H (\mathbf{n}_{S,n,m}^{DS}) / d_{n,m}^{DS}$ are the equivalent noises.

After M_s^D OFDM symbols at N_c^D subcarriers are transmitted, we obtain echo signal matrices $\hat{\mathbf{H}}_{S1}^{DS}$ and $\hat{\mathbf{H}}_{S2}^{DS}$, where $[\hat{\mathbf{H}}_{S1}^{DS}]_{n,m} = \hat{h}_{S1,n,m}^{DS}$ and $[\hat{\mathbf{H}}_{S2}^{DS}]_{n,m} = \hat{h}_{S2,n,m}^{DS}$. We can see that $\hat{\mathbf{H}}_{S1}^{DS}$ and $\hat{\mathbf{H}}_{S2}^{DS}$ are also composed of range and Doppler steering vectors as shown in (23) and (24). Here, we construct range and Doppler steering vector for DL echo sensing as

$$\begin{aligned} \mathbf{a}_r^D(r) &= \mathbf{a}_r(r; \Delta f^D, N_c^D), \\ \mathbf{a}_f^D(f) &= \mathbf{a}_f(f; T_s^D, M_s^D). \end{aligned} \quad (51)$$

According to **Theorem 1**, we use the noise subspaces of $\frac{1}{M_s^D} \hat{\mathbf{H}}_{S1}^{DS} (\hat{\mathbf{H}}_{S1}^{DS})^H$ and $\frac{1}{M_s^D} \hat{\mathbf{H}}_{S2}^{DS} (\hat{\mathbf{H}}_{S2}^{DS})^H$, denoted by $\mathbf{U}_{x,rN}^{DS1}$ and $\mathbf{U}_{x,rN}^{DS2}$, to construct the range spectrum functions as

$$\begin{aligned} f_{r1}^{DS}(r) &= [\mathbf{a}_r^D(r)]^H \mathbf{U}_{x,rN}^{DS1} (\mathbf{U}_{x,rN}^{DS1})^H \mathbf{a}_r^D(r), \\ f_{r2}^{DS}(r) &= [\mathbf{a}_r^D(r)]^H \mathbf{U}_{x,rN}^{DS2} (\mathbf{U}_{x,rN}^{DS2})^H \mathbf{a}_r^D(r). \end{aligned} \quad (52)$$

We also use the noise subspaces of $\frac{1}{N_c^D} (\hat{\mathbf{H}}_{S1}^{DS})^T (\hat{\mathbf{H}}_{S1}^{DS})^*$ and $\frac{1}{N_c^D} (\hat{\mathbf{H}}_{S2}^{DS})^T (\hat{\mathbf{H}}_{S2}^{DS})^*$, denoted by $\mathbf{U}_{x,fN}^{DS1}$ and $\mathbf{U}_{x,fN}^{DS2}$, to construct the Doppler spectrum functions as

$$\begin{aligned} f_{f1}^{DS}(f) &= [\mathbf{a}_f^D(f)]^H \mathbf{U}_{x,fN}^{DS1} (\mathbf{U}_{x,fN}^{DS1})^H \mathbf{a}_f^D(f), \\ f_{f2}^{DS}(f) &= [\mathbf{a}_f^D(f)]^H \mathbf{U}_{x,fN}^{DS2} (\mathbf{U}_{x,fN}^{DS2})^H \mathbf{a}_f^D(f). \end{aligned} \quad (53)$$

Then, we can use **Algorithm 1** to identify the minimal points of $f_{r1}^{DS}(r)$ and $f_{f1}^{DS}(f)$, and $f_{r2}^{DS}(r)$ and $f_{f2}^{DS}(f)$ as processed in Section III-A2. These minimal points are the estimated range and Doppler results for the targets in directions $\hat{\mathbf{p}}_0^U$ and \mathbf{p}_S^D , respectively. Note that $\nabla_{\mathbf{p}} f(\mathbf{p})$ and

$\mathbf{H}_p(\mathbf{p})$ in **Algorithm 1** are replaced with the inverse value, the first-order and second-order derivatives of $f_{r1}^{DS}(r)$ and $f_{r2}^{DS}(r)$ for range estimation, and those of $f_{f1}^{DS}(f)$ and $f_{f2}^{DS}(f)$ for Doppler estimation, respectively.

The range estimation is denoted by $\Theta_{r1}^{DS} = [\hat{r}_{k1}^{DS}/2]_{k1=0, \dots, N_{x,s1}^D-1}$, and the Doppler estimation is denoted by $\Theta_{f1}^{DS} = [\hat{f}_{k1}^{DS}/2]_{k1=0, \dots, N_{x,s1}^D-1}$. The range and Doppler estimation sets of the targets in direction \mathbf{p}_S^D are denoted by $\Theta_{r2}^{DS} = [\hat{r}_{k2}^{DS}/2]_{k2=0, \dots, N_{x,s2}^D-1}$ and $\Theta_{f2}^{DS} = [\hat{f}_{k2}^{DS}/2]_{k2=0, \dots, N_{x,s2}^D-1}$, respectively, where $N_{x,s1}^D$ and $N_{x,s2}^D$ are the numbers of targets in the corresponding directions, respectively. Then, we match the decoupled range and Doppler estimation results according to **Theorem 2**. The matching matrices can be constructed as

$$\begin{aligned} \mathbf{M}_{rf1}^{DS} &= \|\tilde{\mathbf{A}}_{r1}^{DS} \tilde{\mathbf{H}}_{S1}^{DS} [\tilde{\mathbf{A}}_{f1}^{DS}]^*\|_2^2 \in \mathbb{C}^{N_{x,s1}^D \times N_{x,s1}^D} \\ \mathbf{M}_{rf2}^{DS} &= \|\tilde{\mathbf{A}}_{r2}^{DS} \tilde{\mathbf{H}}_{S2}^{DS} [\tilde{\mathbf{A}}_{f2}^{DS}]^*\|_2^2 \in \mathbb{C}^{N_{x,s2}^D \times N_{x,s2}^D}, \end{aligned} \quad (54)$$

where $\tilde{\mathbf{A}}_{r1}^{DS} = [\mathbf{a}_r^D(2r)]_{r1 \in \Theta_{r1}^{DS}}$, $\tilde{\mathbf{A}}_{f1}^{DS} = [\mathbf{a}_f^D(2f)]_{f \in \Theta_{f1}^{DS}}$, $\tilde{\mathbf{A}}_{r2}^{DS} = [\mathbf{a}_r^D(2r)]_{r2 \in \Theta_{r2}^{DS}}$, and $\tilde{\mathbf{A}}_{f2}^{DS} = [\mathbf{a}_f^D(2f)]_{f \in \Theta_{f2}^{DS}}$.

The maximal value of the n th row of \mathbf{M}_{rf} (\mathbf{M}_{rf} can be \mathbf{M}_{rf1}^{DS} or \mathbf{M}_{rf2}^{DS}), e.g., $[\mathbf{M}_{rf}]_{n,m_n}$, indicates the n th point in the range set matches the m_n th point in the Doppler set. Next, Θ_{r1}^{DS} , Θ_{f1}^{DS} , Θ_{r2}^{DS} , and Θ_{f2}^{DS} are rearranged by the matching result.

IV. DUC JCAS DATA FUSION METHOD

In the consecutive UL and DL time slots, due to the channel reciprocity, the relative location and Doppler between BS and the targets, and the UL and DL CSI are treated as unchanged in the block. This section presents the DUC JCAS fusion method for sensing data fusion and communication CSI refining based on this feature.

A. Estimation Feature Acquisition for DUC JCAS

The location of a detected target can be derived, respectively, as

$$\boldsymbol{\Omega} = (r \sin \theta \cos \varphi, r \sin \theta \sin \varphi, r \cos \theta)^T, \quad (55)$$

where r and $\mathbf{p} = (\theta, \varphi)$ are the estimated range and direction, respectively.

In the ULP period, since the LoS path dominates the UL JCAS channel, we only estimate the range and AoA of the user, i.e., $N_{x,s}^U = 1$. The range and AoA of the user are obtained as $\Theta_r^U = [\hat{r}_k^U]_{k=0}$ and $\hat{\mathbf{p}}_0^U$, respectively, and the location of user is calculated as $\hat{\boldsymbol{\Omega}}_0^U$ as shown in (55). In the DLD period, the range and AoA results of the targets in DoU are $\Theta_{r1}^{DS} = [\hat{r}_{k1}^{DS}/2]_{k1=0, \dots, N_{x,s1}^D-1}$ and $\hat{\mathbf{p}}_0^U$, respectively, and we calculate the location of the k_1 th target as $\hat{\boldsymbol{\Omega}}_{k1}^{DS}$; the range and AoA results of the targets in DoI are $\Theta_{r2}^{DS} = [\hat{r}_{k2}^{DS}/2]_{k2=0, \dots, N_{x,s2}^D-1}$ and \mathbf{p}_S^D , and the location of the k_2 th target is calculated as $\hat{\boldsymbol{\Omega}}_{k2}^{DS}$.

Choose the location and Doppler as the feature set for the sensing targets. The feature set for ULP JCAS targets is $\Phi^U = \{\hat{\boldsymbol{\Omega}}_k^U, \hat{f}_k^U\}_{k=0}$, the feature set for ULD JCAS

targets in DoU is $\Phi_1^{DS} = \{\hat{\boldsymbol{\Omega}}_{k1}^{DS}, \hat{f}_{k1}^{DS}\}_{k1=0, \dots, N_{x,s1}^D-1}$, and the feature set for ULD JCAS targets in DoI is $\Phi_2^{DS} = \{\hat{\boldsymbol{\Omega}}_{k2}^{DS}, \hat{f}_{k2}^{DS}\}_{k2=0, \dots, N_{x,s2}^D-1}$.

B. DUC JCAS Sensing Data Fusion Method

Notice that Φ^U is the sensing result of the user, while Φ_1^{DS} is the sensing results, including the user and other dumb targets. Therefore, we can distinguish between the user and other targets by comparing the points in Φ_1^{DS} and Φ^U .

We first give a normalized distance measurement between two estimation feature sets, denoted by $\Phi_1 = \{\boldsymbol{\Omega}_{k1}, f_{k1}\}_{k1=1, \dots, K1}$ and $\Phi_2 = \{\boldsymbol{\Omega}_{k2}, f_{k2}\}_{k2=1, \dots, K2}$. The location and Doppler Euclidean distance matrices between Φ_1 and Φ_2 are given as $\mathbf{Z}_{loc} \in \mathbb{R}^{K1 \times K2}$ and $\mathbf{Z}_f \in \mathbb{R}^{K1 \times K2}$, respectively, with $[\mathbf{Z}_{loc}]_{k1,k2} = \|\boldsymbol{\Omega}_{k1} - \boldsymbol{\Omega}_{k2}\|_2^2$ and $[\mathbf{Z}_f]_{k1,k2} = \|f_{k1} - f_{k2}\|_2^2$. Then, we construct the normalized distance matrix as

$$\mathbf{Z} = \mathbf{Z}_{loc} / [\mathbf{Z}_{loc}]_{\max} + \mathbf{Z}_f / [\mathbf{Z}_f]_{\max}, \quad (56)$$

where $[\mathbf{Z}_{loc}]_{\max}$ and $[\mathbf{Z}_f]_{\max}$ are the maximum values of \mathbf{Z}_{loc} and \mathbf{Z}_f , respectively; and $[\mathbf{Z}]_{i,j} \in [0, 2]$ for all the elements of \mathbf{Z} .

In the high signal-to-noise ratio (SNR) regime, since the estimation mean square error (MSE) of a target is much smaller than the square distance between two different targets, according to the maximum likelihood (ML) criterion, the point-pair between Φ_1 and Φ_2 with the least distance shall be matched as the same target [18]. Therefore, if the minimum value of the k th row of \mathbf{Z} is $[\mathbf{Z}]_{k,l}$, then the k th point of Φ_1 matches the l th point of Φ_2 .

Replace Φ_1 and Φ_2 with Φ^U and Φ_1^{DS} , and then the matched point is the user, while the rest are the dumb points. The matched points in Φ^U and Φ_1^{DS} can be treated as independent estimates of the same parameters. Therefore, the sensing results of a matched point pair can be fused to generate more accurate sensing results. The sensing data fusion method can be developed based on **Theorem 4**.

Theorem 4. Two independent estimates of the same target are denoted by $\mathbf{v}_1 = \mathbf{v} + \Delta \mathbf{v}_1$ and $\mathbf{v}_2 = \mathbf{v} + \Delta \mathbf{v}_2$, respectively, where \mathbf{v} is the actual value, $\Delta \mathbf{v}_1$ and $\Delta \mathbf{v}_2$ are errors that follow Gaussian distributions [15] with $\mathbf{0}$ -mean and variance $E\{\|\Delta \mathbf{v}_1\|_2^2\} = \sigma_1^2$ and $E\{\|\Delta \mathbf{v}_2\|_2^2\} = \sigma_2^2$, respectively. The fusion sensing result is $\bar{\mathbf{v}} = \mathbf{v}_1 + \alpha(\mathbf{v}_2 - \mathbf{v}_1)$ ($0 < \alpha < 1$). Then, the optimal α , denoted by α^* , that minimizes $E\{\|\bar{\mathbf{v}}\|_2^2\}$ is $\alpha^* = \frac{\sigma_1^2}{\sigma_1^2 + \sigma_2^2}$. The minimum of $E\{\|\bar{\mathbf{v}}\|_2^2\}$ is $\frac{\sigma_1^2 \sigma_2^2}{\sigma_1^2 + \sigma_2^2}$.

Proof. The proof is provided in **Appendix D**. \square

According to **Theorem 4**, we can merge the sensing results, including range and velocity, based on the estimation MSE of them. In practical applications, the estimation MSE is not easy to derive directly, we alternatively use Cramer-Rao lower bound (CRLB), i.e., the lower bound for estimation MSE. Moreover, the sensing CRLB is typically inversely proportional to the sensing SNR in the high SNR regime [19], hence we can use the inverse of sensing SNR to replace

sensing CRLB to form a weighted sum of the sensing results in **Theorem 4**.

The sensing SNR can be derived using the eigenvalues of $\hat{\mathbf{H}}_{CS}^U (\hat{\mathbf{H}}_{CS}^U)^H$ and $\hat{\mathbf{H}}_{S1}^{DS} (\hat{\mathbf{H}}_{S1}^{DS})^H$ [12]. The eigenvalue matrices of $\hat{\mathbf{H}}_{CS}^U (\hat{\mathbf{H}}_{CS}^U)^H$ and $\hat{\mathbf{H}}_{S1}^{DS} (\hat{\mathbf{H}}_{S1}^{DS})^H$ in descending order are derived as $\Sigma_r^U \in \mathbb{R}^{N_c^U \times 1}$ and $\Sigma_{r1}^{DS} \in \mathbb{R}^{N_c^D \times 1}$, respectively. Here, we derive the sensing SNR of Φ^U as an example. The sensing SNR of the k th point of Φ^U is

$$\gamma_k = ([\Sigma_r^U]_k - \hat{\sigma}_N^U) / \hat{\sigma}_N^U, \quad (57)$$

where $\hat{\sigma}_N^U$ is the estimated noise power and is calculated as the mean value of the last $N_c^U - N_{x,s}^U$ eigenvalues of Σ_r^U . In this way, all the sensing SNRs of detection points in Φ^U and Φ_1^{DS} can be estimated, and the inverse of sensing SNRs can be used as the variances in **Theorem 4**.

According to **Theorem 4**, we summarize the matching and fusion method in **Algorithm 2**, and the output fused estimation set is $\bar{\Phi}$. Note that the first point in $\bar{\Phi}$ is the user. Finally, $\bar{\Phi}$ and Φ_2^{DS} are obtained as the sensing results in a round of consecutive UL and DL time slots.

C. DUC Communication CSI Fusion Method

BS stores both the UL CSI estimates and DL CSI feedback. Here, we consider the feedback with no quantization error.

According to (22) and (37), we can see that the UL and DL estimated CSI can also be treated as independent observation of the same CSI due to the channel reciprocity. Therefore, **Theorem 4** can also be used to refine the estimated CSI. Since $\|\mathbf{w}_{RX}^D\|_2^2 = \|\mathbf{w}_{RX}^U\|_2^2 = 1$, and $\bar{d}_{n,m}^D$ and $\bar{d}_{n,m}^U$ are the preamble symbols with constant modulus 1, we obtain the variance of $w_{t,n,m}^U$ and $w_{t,n,m}^D$ as $\sigma_1^2 = \frac{\sigma_N^2}{P_t^U} = \frac{1}{\gamma_U}$ and $\sigma_2^2 = \frac{\sigma_N^2}{P_t^D} = \frac{1}{\gamma_D}$, respectively, where γ_U and γ_D are the SNRs for the ULP and DLP communication received signals, respectively.

Construct $\hat{\mathbf{H}}_{CS}^U \in \mathbb{C}^{N_c^U \times M_s^U}$ and $\hat{\mathbf{H}}_{CS}^D \in \mathbb{C}^{N_c^D \times M_s^D}$, where $[\hat{\mathbf{H}}_{CS}^U]_{n,m} = \hat{h}_{CS,n,m}^U$ and $[\hat{\mathbf{H}}_{CS}^D]_{n,m} = \hat{h}_{CS,n,m}^D$. Based on $\hat{\mathbf{H}}_{CS}^U$ and $\hat{\mathbf{H}}_{CS}^D$, we can use the same SNR estimation method in (57) to calculate γ_U and γ_D from the eigenvalues of $\hat{\mathbf{H}}_{CS}^U (\hat{\mathbf{H}}_{CS}^U)^H$ and $\hat{\mathbf{H}}_{CS}^D (\hat{\mathbf{H}}_{CS}^D)^H$, respectively. According to **Theorem 4**, we can fuse the communication CSI based on $\sigma_1^2 = \frac{1}{\gamma_U}$ and $\sigma_2^2 = \frac{1}{\gamma_D}$ as

$$\hat{h}_{CS,n,m}^{DU} = \hat{h}_{CS,n,m}^U + \frac{\sigma_1^2}{\sigma_1^2 + \sigma_2^2} (\hat{h}_{CS,n,m}^D - \hat{h}_{CS,n,m}^U). \quad (58)$$

Next, the demodulated communication received symbol is

$$\tilde{d}_{n,m}^i = \frac{y_{C,n,m}^i}{\sqrt{P_t^i} \hat{h}_{CS,n,m}^{DU}}, \quad (59)$$

where $i = U$ or D are for UL and DL demodulation, respectively; $y_{C,n,m}^i = (\mathbf{w}_{RX}^i)^H \mathbf{y}_{C,n,m}^i$ is the received data signal after BF, and $\mathbf{y}_{C,n,m}^i$ is given in (8). Based on the ML criterion, the UL and DL communication data can be decoded as

$$\hat{d}_{n,m}^i = \arg \min_{d \in \Theta_{QAM}} \left\| \tilde{d}_{n,m}^i - d \right\|_2^2, \quad (60)$$

where Θ_{QAM} is the used QAM constellation.

Algorithm 2: DUC JCAS Sensing Data Fusion Method

Input: The sensing results set Φ^U and Φ_1^{DS} .

Output: The fused DUC JCAS estimation set $\bar{\Phi}$.

Step 1: Count the numbers of points in Φ^U and Φ_1^{DS} as K_1 and K_2 , respectively, calculate the normalized distance matrix between Φ^U and Φ_1^{DS} by applying (56) as \mathbf{Z} , and generate a null set $\bar{\Phi}$.

Step 2: for $k = 1$ to K_1 **do**

$ind_l = \arg \min_l [\mathbf{Z}]_{k,l}$;

Fuse the k th point of Φ^U with the ind_l th point of Φ_1^{DS} by applying **Theorem 4**;

Put the fused results into set $\bar{\Phi}$;

end

Step 3: The remaining points in Φ_1^{DS} that are not matched, are finally put into $\bar{\Phi}$.

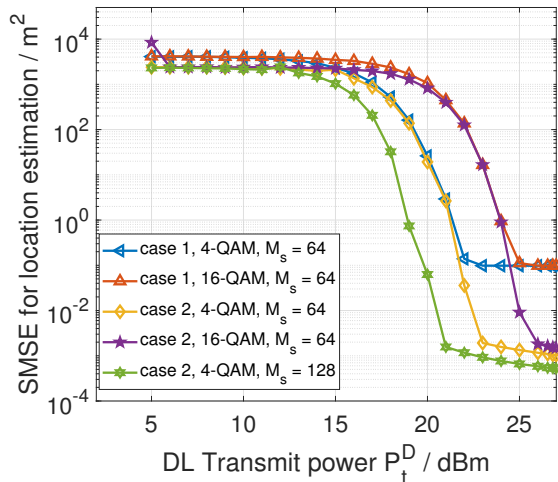
return $\bar{\Phi}$.

V. SIMULATION RESULTS

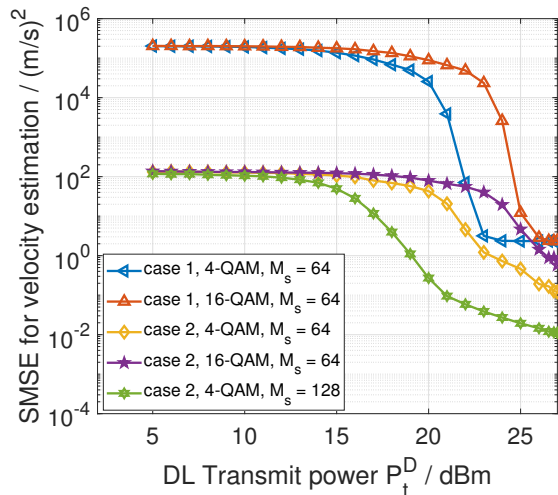
In this section, we present the sensing and communication performance of the proposed DUC JCAS. For comparison, we also plot the sensing and communication performance of the conventional separated UL and DL JCAS, where BS only senses the environment in a single time slot with an on-grid sensing scheme [11]. The simulation parameters are listed as follows.

The carrier frequency is set to 63 GHz [20], the antenna interval, d_a , is half the wavelength, the sizes of antenna arrays of BS and the user are $P_t \times Q_t = 8 \times 8$ and $P_r \times Q_r = 1 \times 1$, respectively. The subcarrier interval is $\Delta f^U = \Delta f^D = \Delta f = 480$ kHz, the subcarrier numbers for UL and DL JCAS are set to $N_c^D = N_c^U = N_c = 256$, and the bandwidth for JCAS is $B = N_c \Delta f = 122.88$ MHz. The OFDM symbols used for UL and DL JCAS are set to be the same, i.e., $M_s^U = M_s^D = M_s$. The variance of the Gaussian noise is $\sigma_N^2 = kFTB = 4.9177 \times 10^{-12}$ W, where $k = 1.38 \times 10^{-23}$ J/K is the Boltzmann constant, $F = 10$ is the noise factor, and $T = 290$ K is the standard temperature. The maximum DL and UL transmit power are $P_t^D = 27$ dBm and $P_t^U = 20$ dBm. The locations of BS and the user are (50, 4.75, 7) m and (140, 0, 2) m, respectively. The location of the scatterer in DoU is (132, 4.5, 3) m, and the location of the target in DoI is (120, 20, 7) m. Moreover, we set the reflection factors of the targets are $\sigma_{C,\beta,l}^2 = \sigma_{S,\beta,l}^2 = 1$. The velocity of the scatterer in DoI is (−40, 0, 0) km/h, and the velocities of the BS and user are (0, 0, 0) m/s. Note that the above locations and velocities of UE and scatterers are only used for generating some parameters in the simulation setup according to Section II-D, and they are unknown to BS. Then, the range, relative velocity, and location of the UE and targets can be estimated by applying the proposed DUC JCAS signal processing scheme.

The estimation MSEs of range, velocity, and location are defined as the mean values of the squared error of all the estimates, respectively. The velocity is calculated as $\hat{v} = \lambda \hat{f}_d$, where \hat{f}_d is the estimated Doppler of the target, and λ is the wavelength. To measure the sensing performance of estimating

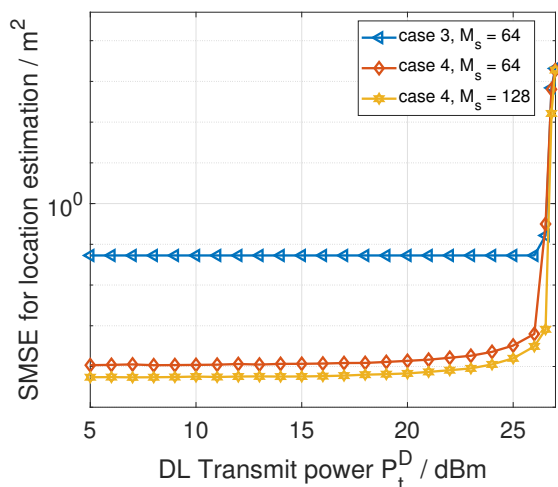


(a) Location estimation SMSEs of cases 1 and 2.

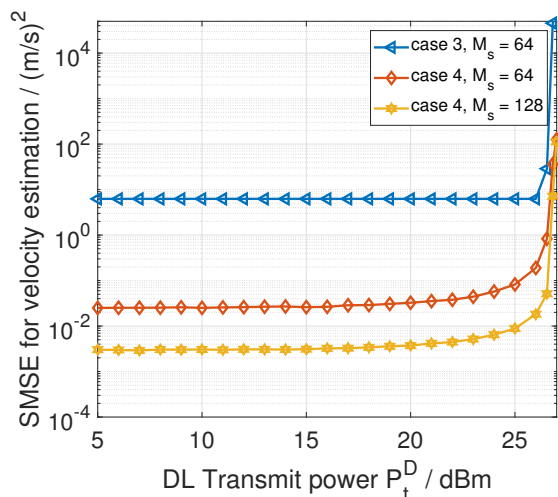


(b) Radial velocity estimation SMSEs of cases 1 and 2.

Fig. 4: The location and radial velocity estimation SMSEs of cases 1 and 2.



(a) Location estimation SMSEs of cases 3 and 4.



(b) Radial velocity estimation SMSEs of cases 3 and 4.

Fig. 5: The location and radial velocity estimation SMSEs of cases 3 and 4.

all the targets mentioned above, we use the sum of the estimation MSEs of all the targets in specified directions as the sensing performance, which is named the sum of MSEs (SMSE). To simplify the demonstration, we predefine 6 cases, which are listed as follows:

Case 1: The estimation SMSE of the targets in DoU with conventional separated DL and UL JCAS in [11].

Case 2: The estimation SMSE of the targets in DoU with the proposed DUC JCAS.

Case 3: The estimation SMSE of the targets in DoI with conventional separated DL and UL JCAS in [11].

Case 4: The estimation SMSE of the targets in DoI with the proposed DUC JCAS.

Case 5: The estimation SMSE of all the targets with conventional separated DL and UL JCAS in [11].

Case 6: The estimation SMSE of all the targets with the proposed DUC JCAS.

A. Sensing Performance

Figs. 4(a) and 4(b) present the location and radial velocity estimation SMSEs of cases 1 and 2. As P_t^D increases, the sensing SNR in DoU increases, which leads to the decrease in the location and velocity estimation SMSEs of cases 1 and 2. Given the same M_s and QAM order, we see that the location and velocity estimation SMSEs of case 2 are lower than those of case 1 since the proposed DUC JCAS fuses the DL and UL off-grid super-resolution estimation results to enhance the sensing accuracy. Given $M_s = 64$, the higher QAM order leads to higher SMSEs for both cases 1 and 2. This is because the higher QAM order causes larger equivalent noise as shown

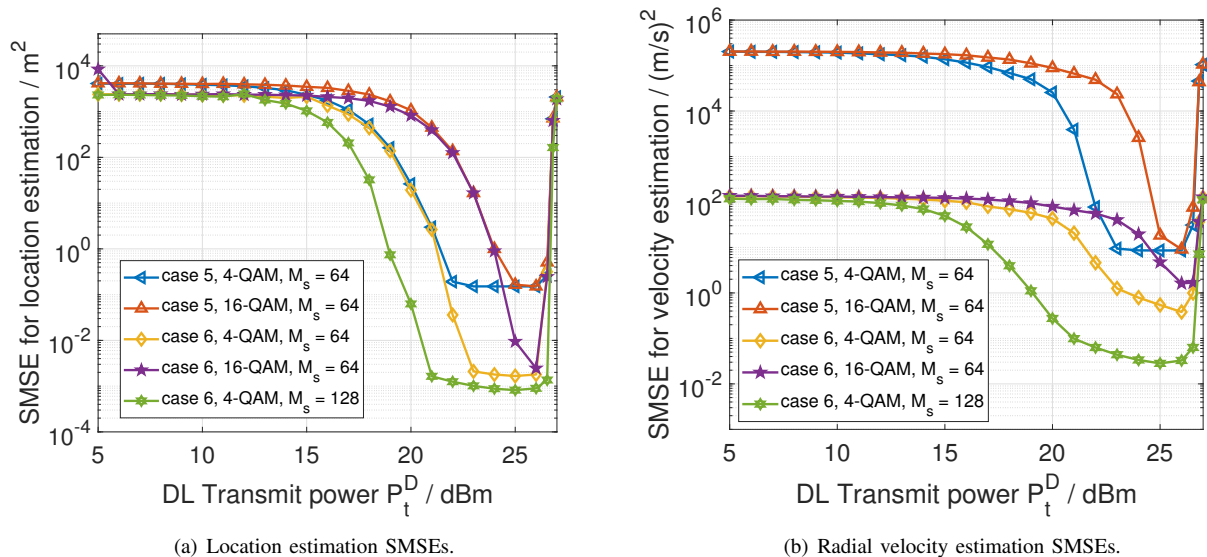


Fig. 6: The location and radial velocity estimation SMSEs of *cases* 5 and 6 under different QAM orders and M_s .

in (49) and (50). Given the same QAM order, the estimation SMSEs of *case 2* under the larger M_s become smaller, because more OFDM symbols result in more energy for sensing as shown in (14) and (52).

Figs. 5(a) and 5(b) show the location and radial velocity estimation SMSEs of *cases* 3 and 4. The increase of P_t^D leads to the decrease of P_t^{DS} as shown in (9), and hence the sensing SNR in DoI decreases, thereby increasing the SMSEs of location and velocity estimations for *cases* 3 and 4. Given the same M_s , the SMSEs of *case 4* is lower than *case 3*, benefiting from the off-grid super-resolution estimation ability of DUC JCAS. Moreover, the SMSEs decrease with the growth of M_s for *case 4* as more energy is accumulated for sensing when more OFDM symbols are used.

Figs. 6(a) and 6(b) show the location and velocity estimation SMSEs of *cases* 5 and 6 under different QAM orders and M_s . The estimation SMSEs of *cases* 5 and 6 are the sum of *cases* 1 and 3, and the sum of *cases* 2 and 4, respectively. Therefore, as P_t^D increases, the location and velocity estimation SMSEs decrease at first, then increase to a large value when P_t^{DS} becomes too small. Given the same QAM order and M_s , the SMSEs of *case 6* are about 20 dB lower than those of *case 5* because the proposed DUC JCAS can fuse the DL and UL off-grid super-resolution estimation results to enhance sensing performance. Given the same QAM order, the increase of M_s leads to a decrease in estimation SMSEs. This is because the aggregate energy used for sensing increases as M_s increases. The increase of M_s makes the velocity estimation SMSE decrease by more percent than the location estimation SMSE. Specifically, the required P_t^D to achieve the same location estimation SMSE is about 2 dBm lower for *case 6* with $M_s = 128$ than that with $M_s = 64$, while the decrease of required P_t^D is about 3 dBm to achieve the same velocity estimation SMSE. This is because the increase of M_s directly increases the length of symbol time, which leads to the higher Doppler

accuracy.

B. Communication Performance

In our proposed DUC JCAS schemes, BS and UE demodulate the communication data with the refined CSI, $\hat{h}_{CS,n,m}^{DU}$, as shown in (58). By comparison, the conventional separated DL and UL JCAS system uses the CSI estimated in one DLP or ULP frames, i.e., (22) or (37), to demodulate the communication data. In this subsection, we simulate communications using these two schemes, respectively. The number of trials for generating each result is $N_{cir} = 10^4$.

Fig. 7 shows BERs of the proposed DUC JCAS and the conventional separated DL and UL communication under 4-QAM and 16-QAM. As P_t^D increases, BER decreases. Given the same QAM order, the BER of the proposed DUC JCAS is lower than that of the conventional communication scheme. This is because DUC JCAS can fuse the estimated CSI in ULP and DLP periods to generate a more accurate CSI. Particularly, the BER gap between these two schemes with 16-QAM modulation is larger than that with 4-QAM modulation, because the higher QAM order is more sensitive to CSI estimation errors, leading to the larger BER gap.

VI. CONCLUSION

In this paper, we propose a DUC JCAS scheme and corresponding DUC JCAS signal processing scheme, which includes a unified UL and DL JCAS sensing scheme and a DUC JCAS fusion method. The unified UL and DL JCAS sensing scheme can achieve off-grid super-resolution estimation for AoA, range, and Doppler with a MUSIC-based sensing processing module. By leveraging the correlation between UL and DL JCAS channels, the DUC JCAS fusion method can distinguish between the sensing results of the user and other dumb scatterers, improving the sensing accuracy. By exploiting the channel reciprocity in the consecutive UL and

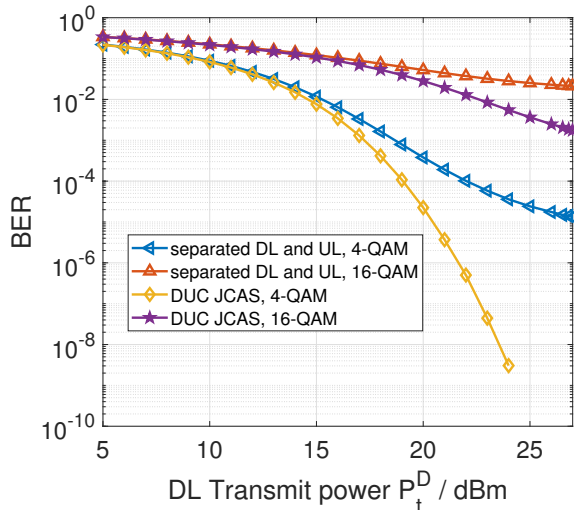


Fig. 7: The BERs of the proposed DUC JCAS and the conventional separated DL and UL communication, under 4-QAM and 16-QAM.

DL timeslots, the DUC JCAS signal processing scheme can refine the estimated CSI and achieves higher communication reliability.

APPENDIX A PROOF OF THEOREM 2

We note that \mathbf{A}_r and \mathbf{A}_f are composed of exponential functions, i.e., $e^{-j2\pi n\Delta f \frac{r_l}{c}}$ and $e^{j2\pi m T_s f_l}$. We can obtain that the maximum value of $\|[\mathbf{a}_r(r)]^H \mathbf{A}_r \mathbf{S} \mathbf{S}^H (\mathbf{A}_f)^T [\mathbf{a}_f(f)]^*\|_2^2$ is $N_c M_s$, which is located at $(r = r_l, f = f_l)$, $l = 0, 1, \dots, L - 1$. Further, since \mathbf{S} is a diagonal matrix with diagonal elements independent of \mathbf{A}_r and \mathbf{A}_f , when $(r = r_l, f = f_l)$, $\|[\mathbf{a}_r(r)]^H \mathbf{A}_r \mathbf{S} \mathbf{S}^H (\mathbf{A}_f)^T [\mathbf{a}_f(f)]^*\|_2^2$ can achieve the local maximum.

APPENDIX B PROOF OF THEOREM 3

According to the feature of mono-static active sensing, for \mathbf{H}_{SU} , only when $\mathbf{p}_S \in \Theta$, BS receives observable echo signals. Otherwise, $(\mathbf{w}_{RX})^H \mathbf{H}_{SU} \mathbf{w}_{TX} \approx 0$ [15]. When $\mathbf{p}_S = \mathbf{p}_{S,\bar{k}} \in \Theta$, there is also $\mathbf{p}_S \notin \{\mathbf{p}_{S,k}\}_{k=0, \dots, \bar{k}-1, \bar{k}+1, \dots, K-1}$, we hence have

$$(\mathbf{w}_{RX})^H \mathbf{H}_{SU} \mathbf{w}_{TX} \approx b_{S,\bar{k}} (\mathbf{w}_{RX})^H \mathbf{a}(\mathbf{p}_{S,\bar{k}}) \mathbf{a}^T(\mathbf{p}_{S,\bar{k}}) \mathbf{w}_{TX}, \quad (61)$$

where $b_{S,\bar{k}}$ is a complex value. Besides, according to (42), we have

$$(\mathbf{w}_{RX})^H \mathbf{H}_{RS} \mathbf{w}_{TX} = b_0 (\mathbf{w}_{RX})^H \mathbf{a}(\mathbf{p}_S) \mathbf{a}^T(\mathbf{p}_S) \mathbf{w}_{TX}, \quad (62)$$

where b_0 is a complex value. By comparing (61) with (62), we have

$$(\mathbf{w}_{RX})^H \mathbf{H}_{RS} \mathbf{w}_{TX} = k_0 (\mathbf{w}_{RX})^H \mathbf{H}_{SU} \mathbf{w}_{TX}, \quad (63)$$

where k_0 is a complex value. Specially, when $\mathbf{p}_S \notin \Theta$, $k_0 \approx 0$. Based on (63), we obtain the conclusions in **Theorem 3**.

APPENDIX C DERIVATION OF (46) AND (47)

From the constraints of the problems (46) and (47), we can conclude that $\mathbf{w}_{n,m}^D$ and $\mathbf{w}_{n,m}^{DS}$ are in the nullspaces of $\mathbf{H}_{RS,n,m}^D$ and $\mathbf{H}_{IS,n,m}^D$, respectively. By applying SVD to $\mathbf{H}_{RS,n,m}^D$ and $\mathbf{H}_{IS,n,m}^D$, we can obtain the nullspace bases from the left singular matrices of $\mathbf{H}_{RS,n,m}^D$ and $\mathbf{H}_{IS,n,m}^D$, denoted by $\mathbf{U}_{RS,n,m}^{DN}$ and $\mathbf{U}_{IS,n,m}^{DN}$, respectively. Then, we obtain

$$\begin{aligned} \mathbf{w}_{n,m}^D &= \mathbf{U}_{RS,n,m}^{DN} \mathbf{m}_2, \\ \mathbf{w}_{n,m}^{DS} &= \mathbf{U}_{IS,n,m}^{DN} \mathbf{m}_3, \end{aligned} \quad (64)$$

where $\|\mathbf{m}_2\|_2^2 = \|\mathbf{m}_3\|_2^2 = 1$. By substituting (64) into the problems (46) and (47), we obtain

$$\begin{aligned} \max_{\mathbf{m}_2} & \|(\mathbf{m}_2)^H (\mathbf{U}_{RS,n,m}^{DN})^H \mathbf{H}_{IS,n,m}^D \mathbf{w}_{TX}^D\|_2^2 \\ \text{s.t.} & \|\mathbf{m}_2\|_2^2 = 1, \end{aligned} \quad (65)$$

and

$$\begin{aligned} \max_{\mathbf{m}_3, \mathbf{m}_1} & \|(\mathbf{m}_3)^H (\mathbf{U}_{IS,n,m}^{DN})^H \mathbf{H}_{RS,n,m}^D \mathbf{V}_{C,n,m}^{DN} \mathbf{m}_1\|_2^2 \\ \text{s.t.} & \|\mathbf{m}_1\|_2^2 = \|\mathbf{m}_3\|_2^2 = 1, \end{aligned} \quad (66)$$

By applying SVD to $(\mathbf{U}_{RS,n,m}^{DN})^H \mathbf{H}_{IS,n,m}^D \mathbf{w}_{TX}^D$ and $(\mathbf{U}_{IS,n,m}^{DN})^H \mathbf{H}_{RS,n,m}^D \mathbf{V}_{C,n,m}^{DN}$, we obtain

$$(\mathbf{U}_{RS,n,m}^{DN})^H \mathbf{H}_{IS,n,m}^D \mathbf{w}_{TX}^D = \mathbf{U}_{IS}^D \Sigma_{IS}^D (\mathbf{V}_{IS}^D)^H, \quad (67)$$

$$(\mathbf{U}_{IS,n,m}^{DN})^H \mathbf{H}_{RS,n,m}^D \mathbf{V}_{C,n,m}^{DN} = \mathbf{U}_{RS}^D \Sigma_{RS}^D (\mathbf{V}_{RS}^D)^H, \quad (68)$$

where Σ_{IS}^D and Σ_{RS}^D are the real-value diagonal matrices with singular values sorted in the descending order, \mathbf{U}_{IS}^D , \mathbf{V}_{IS}^D , \mathbf{U}_{RS}^D , and \mathbf{V}_{RS}^D are the corresponding right and left singular matrices, respectively, and they are all unitary orthogonal matrices. Therefore, the solutions to (65) and (66) are

$$\mathbf{m}_2 = [\mathbf{U}_{IS}^D]_{:,1}, \quad \mathbf{m}_3 = [\mathbf{U}_{RS}^D]_{:,1}, \quad \mathbf{m}_1 = [\mathbf{V}_{RS}^D]_{:,1}. \quad (69)$$

By applying (69) into (40) and (64), we finally obtain (48).

APPENDIX D PROOF OF THEOREM 4

Since $\bar{\mathbf{v}} = (1 - \alpha)\mathbf{v}_1 + \alpha\mathbf{v}_2$, we obtain the problem

$$\begin{aligned} \min_{\alpha} & \bar{\sigma} = (1 - \alpha)^2 \sigma_1^2 + \alpha^2 \sigma_2^2 \\ \text{s.t.} & 0 < \alpha < 1. \end{aligned} \quad (70)$$

As $\frac{\partial \bar{\sigma}}{\partial \alpha} > 0$, the problem is convex. By solving $\frac{\partial \bar{\sigma}}{\partial \alpha} = 0$, we obtain the optimal value of α as $\alpha^* = \frac{\sigma_1^2}{\sigma_1^2 + \sigma_2^2}$. By substituting α^* into (70), the minimum variance is $\frac{\sigma_1^2 \sigma_2^2}{\sigma_1^2 + \sigma_2^2}$.

REFERENCES

- [1] W. Saad, M. Bennis, and M. Chen, "A Vision of 6G Wireless Systems: Applications, Trends, Technologies, and Open Research Problems," *IEEE Network*, vol. 34, no. 3, pp. 134–142, May 2020.
- [2] Z. Feng, Z. Wei, X. Chen, H. Yang, Q. Zhang, and P. Zhang, "Joint Communication, Sensing, and Computation Enabled 6G Intelligent Machine System," *IEEE Network*, vol. 35, no. 6, pp. 34–42, Nov. 2021.
- [3] F. Liu, C. Masouros, A. Petropulu, H. Griffiths, and L. Hanzo, "Joint radar and communication design: Applications, state-of-the-art, and the road ahead," *IEEE Transactions on Communications*, June 2020.

- [4] X. Chen, Z. Feng, Z. Wei, F. Gao, and X. Yuan, "Performance of Joint Sensing-Communication Cooperative Sensing UAV Network," *IEEE Transactions on Vehicular Technology*, vol. 69, no. 12, pp. 15 545–15 556, Dec. 2020.
- [5] C. Sturm and W. Wiesbeck, "Waveform design and signal processing aspects for fusion of wireless communications and radar sensing," *Proceedings of the IEEE*, vol. 99, no. 7, pp. 1236–1259, May 2011.
- [6] J. A. Zhang, X. Huang, Y. J. Guo, J. Yuan, and R. W. Heath, "Multibeam for joint communication and radar sensing using steerable analog antenna arrays," *IEEE Transactions on Vehicular Technology*, vol. 68, no. 1, pp. 671–685, Jan. 2019.
- [7] A. Zhang, M. L. Rahman, X. Huang, Y. J. Guo, S. Chen, and R. W. Heath, "Perceptive Mobile Networks: Cellular Networks With Radio Vision via Joint Communication and Radar Sensing," *IEEE Vehicular Technology Magazine*, vol. 16, no. 2, pp. 20–30, June 2021.
- [8] S. A. Hassani, B. van Liempd, A. Bourdoux, F. Horlin, and S. Pollin, "Joint in-band full-duplex communication and radar processing," *IEEE Systems Journal*, pp. 1–9, July 2021.
- [9] X. Yuan, Z. Feng, J. A. Zhang, W. Ni, R. P. Liu, Z. Wei, and C. Xu, "Spatio-temporal power optimization for mimo joint communication and radio sensing systems with training overhead," *IEEE Transactions on Vehicular Technology*, vol. 70, no. 1, pp. 514–528, Jan. 2021.
- [10] Z. Ni, J. A. Zhang, X. Huang, K. Yang, and J. Yuan, "Uplink sensing in perceptive mobile networks with asynchronous transceivers," *IEEE Transactions on Signal Processing*, vol. 69, pp. 1287–1300, Feb. 2021.
- [11] Y. Liu, G. Liao, Y. Chen, J. Xu, and Y. Yin, "Super-Resolution Range and Velocity Estimations With OFDM Integrated Radar and Communications Waveform," *IEEE Transactions on Vehicular Technology*, vol. 69, no. 10, pp. 11 659–11 672, Aug. 2020.
- [12] X. Chen, Z. Feng, Z. Wei, X. Yuan, P. Zhang, J. Andrew Zhang, and H. Yang, "Multiple signal classification based joint communication and sensing system," *IEEE Transactions on Wireless Communications*, pp. 1–14, Feb. 2023.
- [13] J. A. Zhang, K. Wu, X. Huang, Y. J. Guo, D. Zhang, and R. W. Heath, "Integration of radar sensing into communications with asynchronous transceivers," *IEEE Communications Magazine*, pp. 1–7, Aug. 2022.
- [14] W. H. T. Rodger E. Ziemer, *Principles of Communications*, 7th ed. Wiley, 2014.
- [15] M. A. Richards, J. Scheer, W. A. Holm, and W. L. Melvin, "Principles of modern radar," *SciTech Publishing*, pp. 1–925, 2010.
- [16] Y. S. Cho, J. Kim, W. Y. Yang, and C. G. Kang, *MIMO-OFDM Wireless Communications with MATLAB*. Wiley Publishing, 2010.
- [17] M. Haardt, M. Pesavento, F. Roemer, and M. Nabil El Korso, "Chapter 15 - subspace methods and exploitation of special array structures," in *Academic Press Library in Signal Processing: Volume 3*, A. M. Zoubir, M. Viberg, R. Chellappa, and S. Theodoridis, Eds. Elsevier, 2014, vol. 3, pp. 651–717.
- [18] B. C. Levy, "Principles of signal detection and parameter estimation," *Springer Science & Business Media*, 2008.
- [19] C. G. Shi, S. Salous, F. Wang, and J. J. Zhou, "Modified cramer-rao lower bounds for joint position and velocity estimation of a rician target in ofdm-based passive radar networks," *Radio Science*, vol. 52, no. 1, pp. 15–33, Jan. 2017.
- [20] "Study on evaluation methodology of new Vehicle-to-Everything V2X use cases for LTE and NR," *3GPP TR 37.885 V15.3.0*, 2019.